Published online 15 September 2023 *Nucleic Acids Research, 2023, Vol. 51, No. 19* **10467–10483**
https://doi.org/10.1093/nar/gkad732

OTUD5 limits replication fork instability by organizing chromatin remodelers

Angelo de Vivo[1,†], Hongseon Song[2,†], Yujin Lee[2], Neysha Tirado-Class[1], Anthony Sanchez[1], Sandy Westerheide[1], Huzefa Dungrawala[1] and Younghoon Kee[1,2,*]

[1]Department of Molecular Biosciences, College of Arts and Sciences, University of South Florida, Tampa, FL 33647, USA and [2]Department of New Biology, Daegu Gyeongbuk Institute of Science and Technology (DGIST), 333 Techno-Joongang-daero, Dalseong-gun, Daegu 42988, Republic of Korea

Received May 16, 2023; Revised August 01, 2023; Editorial Decision August 05, 2023; Accepted August 25, 2023

ABSTRACT

Proper regulation of replication fork progression is important for genomic maintenance. Subverting the transcription-induced conflicts is crucial in preserving the integrity of replication forks. Various chromatin remodelers, such as histone chaperone and histone deacetylases are known to modulate replication stress, but how these factors are organized or collaborate are not well understood. Here we found a new role of the OTUD5 deubiquitinase in limiting replication stress. We found that OTUD5 is recruited to replication forks, and its depletion causes replication fork stress. Through its C-terminal disordered tail, OTUD5 assembles a complex containing FACT, HDAC1 and HDAC2 at replication forks. A cell line engineered to specifically uncouple FACT interaction with OTUD5 exhibits increases in FACT loading onto chromatin, R-loop formation, and replication fork stress. OTUD5 mediates these processes by recruiting and stabilizing HDAC1 and HDAC2, which decreases H4K16 acetylation and FACT recruitment. Finally, proteomic analysis revealed that the cells with deficient OTUD5-FACT interaction activates the Fanconi Anemia pathway for survival. Altogether, this study identified a new interaction network among OTUD5-FACT-HDAC1/2 that limits transcription-induced replication stress.

GRAPHICAL ABSTRACT

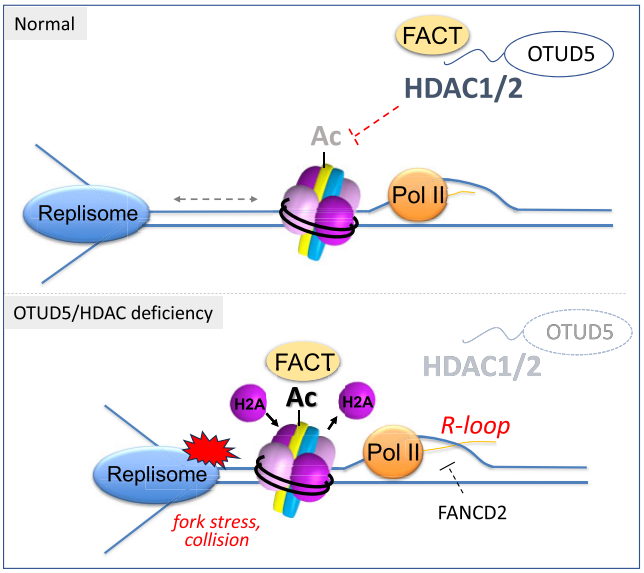

INTRODUCTION

Genomic instability is a hallmark of cancer, aging and many genetic disorders. Genomic instability can be driven by genetic mutations, metabolic alterations or environmental stress. Increasing evidence suggests that transcription can be a significant driver of genomic instability, as improper regulation of the transcriptional process can impede other crucial DNA processes such as DNA replication or repair (1). Cells have evolved mechanisms to suppress transcription-induced genomic aberrations. Transcription-replication conflicts (abbreviated as TRCs) are now considered to be an important source for instability of common fragile sites (CFSs), breakage-prone chromosomal loci that are intimately connected to genomic aberrations and cancer development (2). TRCs can be associated with increased

*To whom correspondence should be addressed. Tel: + 82 53 785 1610; Fax: 82 53 785 1819; Email: ykee@dgist.ac.kr
†The authors wish it to be known that, in their opinion, the first two authors should be regarded as Joint First Authors.

levels of R-loops, a form of RNA–DNA hybrid with a displaced single-stranded DNA, which can cause replication fork stalling and DNA breakages (3). Indeed, a study found that aberrant R-loops are major sources of genomic instability in human cells (4).

Extensive studies in the past several years have elucidated several factors that modulate R-loop formation, TRC, or both. These factors include RECQ5 (5), TOP1 (6–8), THO-SIN3A (9), BRG1 (10), INO80 (11), BMI1-RNF2 (12), SRSF1-3 (13–15), RTEL (16,17), BRD4 (18), PCNA-SUMO (19), ATAD5 (20), Fanconi Anemia proteins (21–26), BRCA1/2 (27–33), CtIP (34) and FACT (35). While these factors are clearly crucial in limiting harmful R-loops that can compromise genomic stability, how these factors are organized spatially or even collaborate, remains relatively unknown.

FACT (*FA*cilitates *C*hromatin *T*ranscription), a heterodimeric complex composed of SSRP1 (Structure-Specific Recognition Protein 1) and SPT16 (Suppressor of Ty 16), is a histone chaperone that plays roles during DNA replication, transcription, and repair (36). FACT assists in disassembly and assembly of nucleosomes ahead of or behind the polymerases, respectively. We previously showed that FACT-mediated transcription contributes to a recovery from a DNA double strand breaks (DSBs), and that this activity is antagonized by the OTUD5-UBR5 complex (37). To understand the consequence of FACT deregulation in a more physiological setting, we used CRISPR knock-in cell lines in which FACT is specifically uncoupled from OTUD5. These cells exhibit higher loading of FACT at chromatin, which is associated with increased replication stress and transcription-replication conflicts. We found that OTUD5-mediates the recruitment and stabilization of two nuclear histone deacetylases, HDAC1 and HDAC2, which balances FACT recruitment and R-loop formations. This work uncovers a new mode of regulation that limits transcription-induced replication fork stress and offers an example of how chromatin remodelers collaborate to prevent genomic instability.

MATERIALS AND METHODS

Cell lines, plasmids and chemicals

HeLa, 293T and HCT116 cells were cultured in Dulbecco's modified Eagle's medium (DMEM) supplemented with 10% fetal bovine serum (FBS). HeLa CRISPR-Cas9 UBR5 KO and OTUD5 KO cell lines were generated using the CRISPR-Cas9 plasmid (purchased from Santa Cruz Biotechnology) and the Double Nickase (Cas9 D10A) OTUD5 KO cell lines were generated using the Double Nickase plasmid purchased from SantaCruz. The cells were transfected with plasmids and transiently selected with puromycin (1μg/ml) for 48 h and surviving cells were isolated into single cells and allowed to grow. HeLa and HCT116 OTUD5^{D537A} knock-in clones and FLAG-SPT16 knock-in 293T clones were generated by the Genome Engineering & iPSC Center (Washington University School of Medicine) using CRISPR guided by gRNA. Genomic mutations were verified by sequencing the loci. OTUD5 cDNA was cloned into p3xFlag-CMV, pBabe-puro and pGEX 6p-1. pyCAG_RNaseH1_WT and D210N plasmids were gifts from Dr Xiang-Dong Fu through Addgene. Hydroxyurea and Aphidicolin were purchased from Fisher Scientific. The ATR inhibitor (AZ20) and Bleomycin were purchased from Selleck Chemical. MG-132 was purchased from AG scientific. Cycloheximide was purchased from Merck.

DNA fiber analysis

Fiber labeling analyses was performed as described previously (Jackson and Pombo 1998: PMID: 9508763). Briefly, cells were pulsed sequentially with 20 μM CldU and 100 μM IdU for 30 min each. Cells were harvested, combined with lysis buffer and spread by tilting the slides. Following fixation and overnight storage at –20°C, DNA was denatured using 2.5N hydrochloric acid for 45 min and blocked in 0.1% Triton X-100/PBS solution with 10% goat serum. Stretched DNA fibers were stained with primary antibodies rat monoclonal anti-BrdU (anti-CldU) and mouse anti-BrdU (anti-IdU) for 2 h following which slides were rinsed and stained with secondary antibodies goat anti-rat Alexa Fluor 594 and goat anti-mouse Alexa Fluor 488 for 1 h. After drying, slides were mounted with Prolong Gold and analyzed using fluorescence microscopy.

Western blots and antibodies

Cell extracts were run on sodium dodecyl sulfate polyacrylamide gel electrophoresis (SDS-PAGE) gels and then transferred to a PVDF membrane (BioRad). Membranes were probed with primary antibodies overnight at 4°C, followed by incubation with HRP-conjugated secondary antibodies (Cell Signaling Technologies) for 1 h. The bound antibodies were viewed via Pierce ECL Western Blotting Substrate (Thermo Scientific). The following primary antibodies were used: α-SPT16, SSRP1, UBR5, OTUD5, HDAC1, HDAC2, HDAC3, HDAC4, MTA, TRAF3, 53BP1, PCNA, RPA32, p53, β-Actin, V5 and CHD4 rabbit or mouse polyclonal antibodies from Cell Signaling Technologies; α-RNA Pol II (S2-P) rabbit polyclonal antibodies from Abcam; α-FLAG mouse monoclonal antibodies from Sigma Aldrich; α-γH2AX, S9.6 and α-Tubulin mouse monoclonal antibodies from Millipore; α-SPT16, α-Cyclin A, α-FANCD2 and α-GST mouse monoclonal antibodies from Santa Cruz Biotechnologies; and α-H4K16ac rabbit monoclonal antibody from Active Motif.

RNAi

Cells were cultured in medium without antibiotics and transfected once with 20 nM siRNA (final concentration) using the RNAiMAX (Invitrogen) reagent following the manufacturer's protocol. The following siRNA sequences were synthesized by QIAGEN:

UBR5#1	CAGGUAUGCUUGAGAAAUAAU
UBR5#2	GAAUGUAUUGGAACAGGCUACUAUU
SPT16	ACCGGAGUAAUCCGAAACUGA
OTUD5 #1	GGCCGGCUUGGACAAUGAATT
XPG	CUGUACUAAGGAGAAAUGA

The following siRNA sequences were synthesized by Bioneer:

OTUD5 #2	UGACCUUGCUGCAUUCCUU
FANCD2	UGACCUUGCUGCAUUCCUU
BRCA1	CUGAAACCAUACAGCUUCA
HDAC1	CUGACAAGCGCAUCUCGAU
HDAC2	GACGGAAACUGAGCUCAGU

qPCR analysis

PCR experiments were performed on Applied Biosystems QuantStudio3 thermocycler using amfiSure qGreen qPCR master mix (GenDEPOT Q5603-001). qPCR reactions were set up to a final volume of 50 μl using 15 ng of template DNA. The PCR cycles used consisted of a 95°C denaturation step (15 s), followed by annealing and extension steps (1 min) at 60°C. 35 cycles were repeated. Measurements were acquired after every cycle. Quantification was performed using delta Ct values of the untreated sample and the experimental sample for each primer set. Target specificity was confirmed by melt curve analysis as well as end point analysis. Cq confidence of samples quantified was >0.98. Following primer sequences were used:

FRA3B Central FW	5′- tgttggaatgttaactctatcccat -3′
FRA3B Central Rv	5′- atatctcatcaagaccgctgca -3′
FRA3B Distal Fw	5′- caatggcttaagcagacatggt -3′
FRA3B Distal Rv	5′- agtgaatggcatggctggaatg -3′
FRA7H Fw	5′- taatgcgtccccttgtgact -3′
FRA7H Rv	5′- ggcagattttagtccctcagc -3′
FRA16D Fw	5′- gatctgccttcaaagactac -3′
FRA16D Rv	5′- caaccaccatttctcactctc -3′
GAPDH Fw	5′- ccctctggtggtggcccctt -3′
GAPDH Rv	5′- ggcgcccagacacccaatcc -3′

Immunoprecipitation and mass spectrometry analysis

293T or HeLa cells stably expressing the transgene (FLAG -OTUD5) or transiently transfected with plasmids grown to 70–80% confluency were harvested by scraping. The pellets were lysed with lysis buffer (25 mM Tris pH 7.4, 0.5% NP40, 100 mM NaCl, 0.1 mM ethylenediaminetetraacetic acid (EDTA) supplemented with a protease inhibitor cocktail solution) for 10–15 min on ice. The lysates were cleared by centrifuging for 30 min at 14 000 RPM, and 10% of the supernatant was collected for 'input' samples while the remaining volume was incubated overnight with anti-FLAG M2 agarose (Sigma Aldrich) at 4°C while rotating. The M2 beads were washed three times with the lysis buffer before elution by boiling at 95°C for 3 min in 1 × Laemli buffer. 10% SDS gel was used to separate the eluted proteins. After bands containing target protein were excised, the proteins were reduced/alkylated and digested with trypsin in the gel band. Peptides were extracted and desalted with Ziptip C18 tips. A nanoflow ultra high performance liquid chromatograph (RSLC, Dionex, Sunnyvale, CA) coupled to an electrospray bench top orbitrap mass spectrometer (Q-Exactive plus, Thermo, San Jose, CA) was used for tandem mass spectrometry peptide sequencing experiments. The sample was first loaded onto a pre-column (2 cm × 100 μm ID packed with C18 reversed-phase resin, 5 μm, 100Å) and washed for 8 min with aqueous 2% acetonitrile and 0.04% trifluoroacetic acid. The trapped peptides were eluted onto the analytical column, (C18, 75 μm ID × 25 cm, 2 μm, 100Å, Dionex, Sunnyvale, CA). The 120-min gradient was programmed as: 95% solvent A (2% acetonitrile + 0.1% formic acid) for 8 min, solvent B (90% acetonitrile + 0.1% formic acid) from 5% to 15% in 5 min, 15% to 40% in 85 min, then solvent B from 50% to 90% B in 7 min and held at 90% for 5 min, followed by solvent B from 90% to 5% in 1 min and re-equilibrate for 10 min. The flow rate on analytical column was 300 nl/min. Sixteen tandem mass spectra were collected in a data-dependent manner following each survey scan. Both MS and MS/MS scans were performed in Orbitrap to obtain accurate mass measurement using 60 second exclusion for previously sampled peptide peaks. Full scan and MS/MS resolution was set at 70 000 and 17 500, respectively. Protein identifications were assigned through Proteome Discoverer using the UniProt Homo sapiens database. Carbamidomethyl (C) was set as a fixed modification and acetyl (protein N-terminus) and oxidation (M) were set as variable modifications. Trypsin/P was designated as the digestion enzyme with the possibility of two missed cleavages. A mass tolerance of 20 ppm (first search)/4.5 ppm (recalibrated second search) was used for precursor ions while fragment ion mass tolerance was 20 ppm. All proteins were identified at a false discovery rate of <1% at the protein and peptide level.

Chromatin immunoprecipitation

Cells were grown to confluency in 10cm dishes, treated with indicated conditions, and crosslinked with formaldehyde (1.42% final concentration) for 10 min at room temperature. Reactions were quenched using glycine (125 mM final concentration) for 5 min. Cells were washed twice using cold PBS with 0.5 mM PMSF and then harvested by scraping. Collected cells were washed twice by gently resuspending with FA lysis buffer (50 mM HEPES–KOH pH 7.6, 140 mM NaCl, 1% Triton X-100, 0.1% sodium deoxycholate) with Inhibitor proteases cocktail added and allowing 1 min incubation on ice, followed by high-speed centrifugation. Cells were lysed using FA lysis buffer with Inhibitor proteases cocktail added and incubating on ice for 10 min, followed by 8 rounds of sonication with 45% amplitude for 10 s allowing sample to rest on ice for 1 min between rounds. Lysed sample was centrifuged at high speed and 4°C. Supernatant was moved to new tube and each sample was normalized using the Bradford assay. Input sample was frozen and kept at –20°C. 400 μl of FA buffers added to the no antibody samples and IP samples were incubated overnight on a rotator at 4°C. Protein A/G agarose beads were added and allowed to incubate in rotator at 4°C for 2 h. Samples were then washed using FA buffer 3 times by gently resuspending and low speed centrifugation. FA buffer was removed without removing A/G beads and 400uL of ChIP Elution buffer (1% SDS, 100 mM sodium bicarbonate) was added to Input, No Abs, and IP samples and incubated for 1 h on a rotator at room temperature. Samples were then centrifuged at high speed and the supernatant was moved to a new tube. RNase A was added to each elute at a final concentration

of 50 μg/ml and allowed to incubate for 2 h at 65°C. Proteinase K was then added to each sample at a final concentration of 250 μg/ml and allowed to incubate overnight at 65°C. DNA was then purified by using a PCR purification kit (Bioneer) on each sample.

Immunofluorescence and image quantification

Cells were seeded in 12-well plates onto coverslips and treated with the indicated siRNA and DNA damage treatments. For UV irradiation, cells were irradiated with 15–100 J/m^2 UVC (UV Stratalinker 2400), depending on the type of experiments. For inhibitor treatments, the ATR inhibitor (AZ20, 100 nM) was added to the cells for 12 h prior to fixing. Cells were fixed and stained for indicated antibodies following standard procedures. For rescue experiments, cells were fixed and stained with the indicated siRNA for 72 h prior to fixation, and plasmids were transfected 24 h prior to fixation. For cell fixation, coverslips were washed twice with ice-cold PBS and fixed for 10 min in the dark with cold 4% paraformaldehyde. Fixed cells were permeabilized for 5 min with 0.25% Triton X-100 and incubated with primary antibodies (diluted in PBS to 1:300–1:500) for 1–2 h in the dark, then with secondary antibodies (diluted in PBS to 1:1000) for 1 hour in the dark, followed by incubating with Vectashield mounting medium containing DAPI (Vector Laboratories Inc). For enzymatic digestion by RNase H, fixed cells were incubated with RNase H (New England Biolabs), which were diluted to 1:50 in 1× RNase H buffer (New England Biolabs), for 5 h at 37°C. Images were collected by a Zeiss Axiovert 200 microscope equipped with a Perkin Elmer ERS spinning disk confocal imager and a 63×/1.45NA oil objective using Volocity software (Perkin Elmer) or were acquired by a Leica DMi8 microscope with Leica Application Suite (LAS X) software. All fluorescence quantification was performed using ImageJ. Fluorescence quantification for S9.6 intensity was performed using Image J. All the fluorescence channels of interest were imported into Image J to measure the relative fluorescence intensity of manually selected single cells. The raw density measurements were normalized to an arbitrary value of 10 for the highest reading. To count the number of foci in nuclei, full color images were split into blue, red, and green; the blue and red channels were analyzed. Single cells (blue) were selected by using 'Analyze particles' after choosing nuclei by 'Threshold the image' in blue channel, and the number of foci (red) were counted using 'find maxima' in the ImageJ.

Proximity ligation assay

Proximity ligation assays were performed using the Duolink kit from Sigma Aldrich; cells were grown in a 12-well format on coverslips. Cells were fixed and permeabilized according to the standard immunofluorescence protocol as previously described (12). Primary antibodies were added at a 1:500 dilution in PBS and incubated for 1 hour at room temperature. Proximity ligation assay (PLA) minus and plus probes were diluted 1:5 in the provided dilution buffer, 30 μl of the probe reaction was added to each coverslip and incubated for 1 h at 37°C; the coverslips were then washed twice with buffer A. The provided ligation buffer was diluted 1:5 in water, and then, the ligase was added at a 1:30 dilution; followed by incubation at 37°C for 30 min before washing twice with wash buffer A. The provided amplification buffer was diluted 1:5 in water before adding the provided polymerase at a 1:80 ratio, the amplification reaction was left at 37°C for 100 min, the reaction was quenched by washing twice with buffer B. The coverslips were mounted on slides with DAPI containing mounting medium. For EdU-PLA, cells were treated with indicated siRNA for 72 h, cells were incubated with EdU (final concentration 10μM) for 12 min before fixing with 4% paraformaldehyde for 10 min, then cells were permeabilized with 0.25% Triton X-100 for 10 min followed by washing with cold PBS. EdU was conjugated with biotin-azide by the Click reaction. Click reaction buffer (2 mM copper sulfate, 10 μM biotin azide, 100 mM sodium ascorbate) was prepared fresh and applied to the slides for 30 min at room temperature. After two PBS washes, cells on the slides were incubated with α-biotin or the indicated antibodies diluted in PBS. Cells were washed with PBS twice. PLA reactions were performed as described above.

Clonogenic survival assay

HeLa, HCT116 and U2OS cells were seeded into 24-well plates (100 cells per well) and treated with the indicated siRNAs for 48 h, then treated with the indicated drugs with indicated concentrations, then allowed to grow for 10–14 days. The plating efficiencies (the number of cells that survive in the absence of drug treatment) were roughly equal between the groups. The cells were fixed with 10% methanol, 10% acetic acid solution for 15 min at room temperature. After crystal violet staining, the cells were dissolved with Sorensen buffer (0.1M sodium citrate, 50% ethanol), then the colorimetric intensity of each solution was quantified using Gen5 software on a Synergy 2. Error bars are representative of three independent experiments.

Protein purification and *in vitro* binding assay

OTUD5 cDNA was cloned into the pGEX-6p vector and transformed into the *Escherichia coli*. BL21 strain. Protein expression was induced by addition of IPTG at a final concentration of 300 μM for 4 h. Cells were harvested and lysed using the ice-cold lysis buffer (150 mM NaCl, 1% Triton, 20 mM Tris pH 7.4, 0.1% EDTA, supplemented with PMSF and protease inhibitor cocktail) while rotating in 4°C. Resuspended pellets were sonicated for three rounds (40 s per pulse), and the lysate was cleared by centrifugation (20 000 RPM for 40 min). Glutathione beads (GE Healthcare) were added to the supernatant and incubated by rotating for 2 h at 4°C. Beads were then washed three times with lysis buffer. Purified proteins were mixed with whole cell lysate from 293T cell and allowed to incubate for 2 h by rotating at 4°C. Beads were washed with lysis buffer (25 mM Tris pH 7.4, 0.5% NP40, 100 mM NaCl, 0.1 mM ethylenediaminetetraacetic acid (EDTA) supplemented with protease inhibitor cocktail solution), then mixed with 2× Laemmli buffer.

RESULTS

UBR5-OTUD5 complex mitigates DNA replication fork stress

While investigating the cellular phenotypes of OTUD5 depletion, we noticed that OTUD5 knockdown causes increased frequency of 53BP1 foci (Figure 1A). This increase in foci is more pronounced in Cyclin A-negative G1 cells, suggesting that these are 53BP1-containing nuclear bodies, which are outcomes of DNA replication stress. The 53BP1-NBs are enriched in common fragile sites (CFSs) of the genome in the wake of replication stress (38). Consistent with this, anti-53BP1 ChIP assays found that 53BP1 is enriched at selected CFSs (FRA3B, FRA16D, FRA7H are prominent CFSs that become fragile upon replication stress in various cell types(12)) in OTUD5 knockdown cells, compared to control cells (Figure 1B). Consistent with the increased replication stress incurred by OTUD5 depletion, Proximity Ligase Assays (PLA) showed that single strand binding protein RPA is more increased at nascent forks (labeled by EdU) upon OTUD5 depletion (Figure 1C). OTUD5 and UBR5 depletion caused increased formation of micronuclei, which often results from replication stress (Figure 1D), and increased sensitivity to hydroxyurea (Figure 1E), another indication of increased replication stress. Anti-OTUD5 ChIP assay found that OTUD5 proteins themselves are enriched in CFSs upon HU treatment (Figure 1F). Consistently, PLA found that OTUD5 and UBR5 proteins are present at nascent forks, with slight increases upon HU treatment (Figure 1G). Altogether, these results suggest that OTUD5, and its binding partner UBR5, are mitigators of DNA replication fork stress.

UBR5-OTUD5 complex mitigates transcription-replication conflicts

We hypothesized that the OTUD5-UBR5 complex may mitigate TRCs, based on our previous finding that the OTUD5-UBR5 complex regulates DNA double strand break (DSB)-induced transcription arrest, and that OTUD5-UBR5 proteins are present at replication forks (Figure 1G). Using a PLA-based readout for TRC (4), we found that OTUD5 or UBR5 depletion causes increased proximity of PCNA and an elongating form of RNA polymerase II (RNA Pol II (S2-P)) (Figure 2A). RNA Pol II (S2-P) is more present in nascent forks (EdU) upon OTUD5 or UBR5 depletion (Figure 2B), consistently arguing that TRC incidences are increased in OTUD5- or UBR5-depleted cells. TRCs are associated with increased DNA–RNA hybrids (4). Consistent with this notion, we found that DNA–RNA hybrids are increased in OTUD5 or UBR5-depleted cells (Figure 2C), as detected by the monoclonal S9.6 antibodies. The level of DNA–RNA hybrids caused by OTUD5 or UBR5 depletion is slightly lower than those caused by SPT16 or FANCD2 depletion, two conditions known to cause accumulation of DNA–RNA hybrids (21,22,35). The increased S9.6 signals are partially reduced by expressing V5-tagged RNase H1 (RNH1) in the cells, which preferentially removes R-loops (39,40), confirming that a substantial fraction of the S9.6 signals in these cells represent R-loops. We noticed that overexpressing RNH1 itself causes a slight increase in the S9.6 signal in control cells, a phenomenon also seen in previous literatures - which could be due to increased replicative stress or DNA damage associated with overexpressing RNH1 (9,41). To test if the R-loops accumulate in CFSs, we performed ChIP assays using the S9.6 antibody and found that the R-loops are significantly enriched in selected CFSs in OTUD5 or UBR5 CRISPR knockout cells (on average 5–6 folds, Figure 2D). Catalytically inactive RNH1 (D210N) can bind to R-loops with increased affinity (39). Anti-V5-RNH1 D210N ChIP indeed showed that the mutant RNH1 proteins are more enriched in CFSs in OTUD5-depleted cells (Figure 2E), confirming the results with S9.6 antibodies. Increased TRCs and R-loop formations can be caused by, or lead to, transcription stress, which is reflected by increased occupancy of RNA polymerases (42). Consistent with this notion, anti-RNA Pol II (S2-P) ChIP showed an increased presence of RNA Pol II (S2-P) at the CFSs in OTUD5 knockdown cells (Figure 2F). Altogether, these data suggest that OTUD5 and UBR5 mitigate the incidence of TRCs and R-loop formations.

Uncoupling FACT from OTUD5 leads to replication stress

We have previously shown that the FACT histone chaperone, necessary for remodeling nucleosomes to allow for transcription, is negatively regulated by OTUD5 upon nuclease induction of DSBs (37). In the study, we identified the OTUD5 point mutation D537A as abrogating the interaction with FACT. The OTUD5 D537A mutation frequently occurs in chronic myeloid leukemia (CML) (per Cbioportal) within the C-terminal disordered region of OTUD5 and results in the failure to support DSB-induced transcription arrest. Interestingly, the OTUD5-FACT interaction also plays an important role in replication stress mitigation, as the OTUD5 D537A mutant did not rescue the G1 body increase in OTUD5 knockdown cells, while its wild-type counterpart did (Supplementary Figure S1). These results imply that the mechanisms involved in DSB-induced transcription arrest also play roles in the context of replication, wherein conflict with transcription can be an obstacle that generates replication stress. To study the cellular consequence of specifically blocking the interaction between OTUD5 and FACT (OTUD5 overexpression or complete knockout causes aberration in cell cycle and apoptosis), we generated a HeLa knock-in (KI) cell line in which the D537A mutation is introduced into the genomic loci of OTUD5 ($OTUD5^{D537A}$) using the CRISPR-Cas9 method (Supplementary Figure S2; sequencing information of 4 clones).

We first confirmed that the protein levels of OTUD5, UBR5, FACT complex subunits (SPT16, SSRP1) are unaffected in the $OTUD5^{D537A}$ KI cells (Supplementary Figure S3). However, anti-SPT16 co-immunoprecipitation showed that the interaction with UBR5 and OTUD5 proteins is lost in the KI cells (Figure 3A). Reverse co-IP (anti-OTUD5 IP) consistently found similar results (Figure 3B). Interaction with TRAF3, a protein known to associate with OTUD5, is unaffected in the KI cells, supporting that the OTUD5-FACT interaction is specifically disrupted in these clones. Disruption of the OTUD5-SPT16 interaction was also confirmed using PLA wherein the PLA signals were

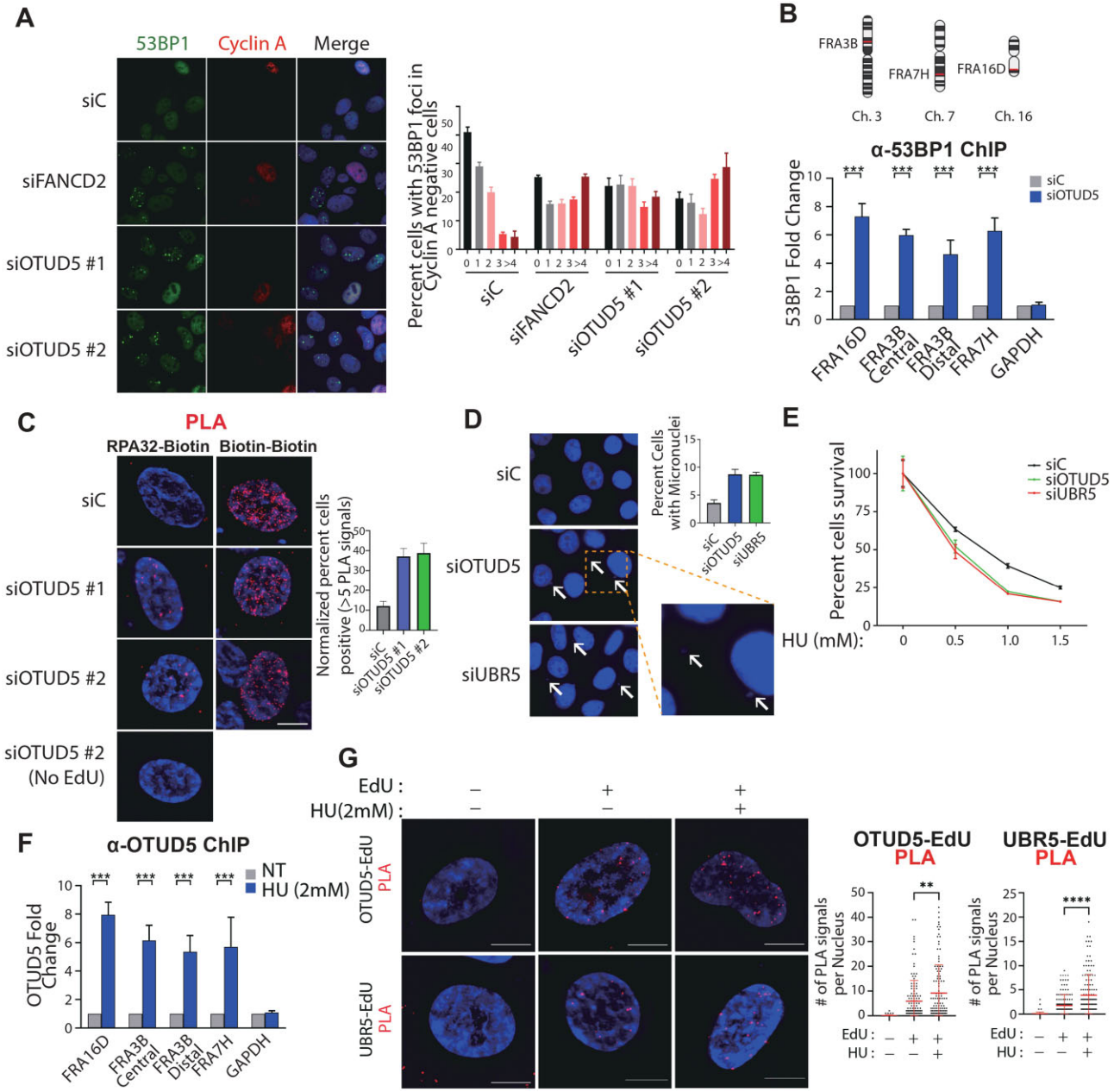

Figure 1. OTUD5 mitigates replication fork stress. (**A**) OTUD5 knockdown leads to DNA replication stress, as indicated by increased frequency of 53BP1 foci. HeLa cells were transfected with the indicated siRNAs (20 nM), and 72 h later cells were fixed and co-stained with 53BP1 (green) and Cyclin A (red) antibodies. On the right is quantification for 53BP1 foci in Cyclin A negative cells. The experiments were conducted in triplicate. The number of foci is counted using ImageJ ($n = 100$ in each). (**B**) 53BP1 is enriched at selected CFSs in OTUD5 knockdown cells. (Top) Schematic for Common fragile site and primer binding location on FRA3B, FRA7H and FRA16D. (Bottom) qPCR quantification of 53BP1 ChIP in HeLa cells transfected with either control or OTUD5 siRNA, the experiments were conducted in triplicate. Statistical analysis was performed using 'one way ANOVA' (***$P < 0.0005$). (**C**) The single strand binding protein RPA is increased at nascent forks upon OTUD5 depletion. (Left) Representative images of PLA signals between EdU and RPA32. The signals are increased in HeLa cells transfected with OTUD5 siRNA. (Right) Quantification of percentage of cells with more than 5 PLA signals, with normalization to biotin–biotin signals. The experiment was conducted in triplicate ($n = 50$ in each experiment). (**D**) OTUD5 and UBR5 depletion causes increased formation of micronuclei. (Left) Representative images of increased micronuclei in HeLa cells depleted of OTUD5 or UBR5 by siRNAs. (Right) Quantification of the percentage of cells with micronuclei ($n = 100$). (**E**) OTUD5 and UBR5 depletion cause increased sensitivity to hydroxyurea. HeLa cells were transfected with indicated siRNAs, then 48 h later treated with indicated concentration of hydroxyurea. Cells were incubated for 10 additional days, fixed then stained by crystal violet. The staining intensities measured by using Gen5 software on a Synergy 2. Assays were performed in triplicates. (**F**) qPCR quantification of OTUD5 ChIP in HeLa cells either untreated or treated with hydroxyurea (2 mM) (***$P < 0.0005$). (**G**) OTUD5 and UBR5 proteins are present at nascent forks. (Left) Representative images of PLA signals between EdU and OTUD5 or UBR5. HeLa cells were labeled with 50μM EdU for 15mins then treated with or without hydroxyurea for 2 h. (Right) Quantification of the PLA signals per nucleus ($n = 100$).

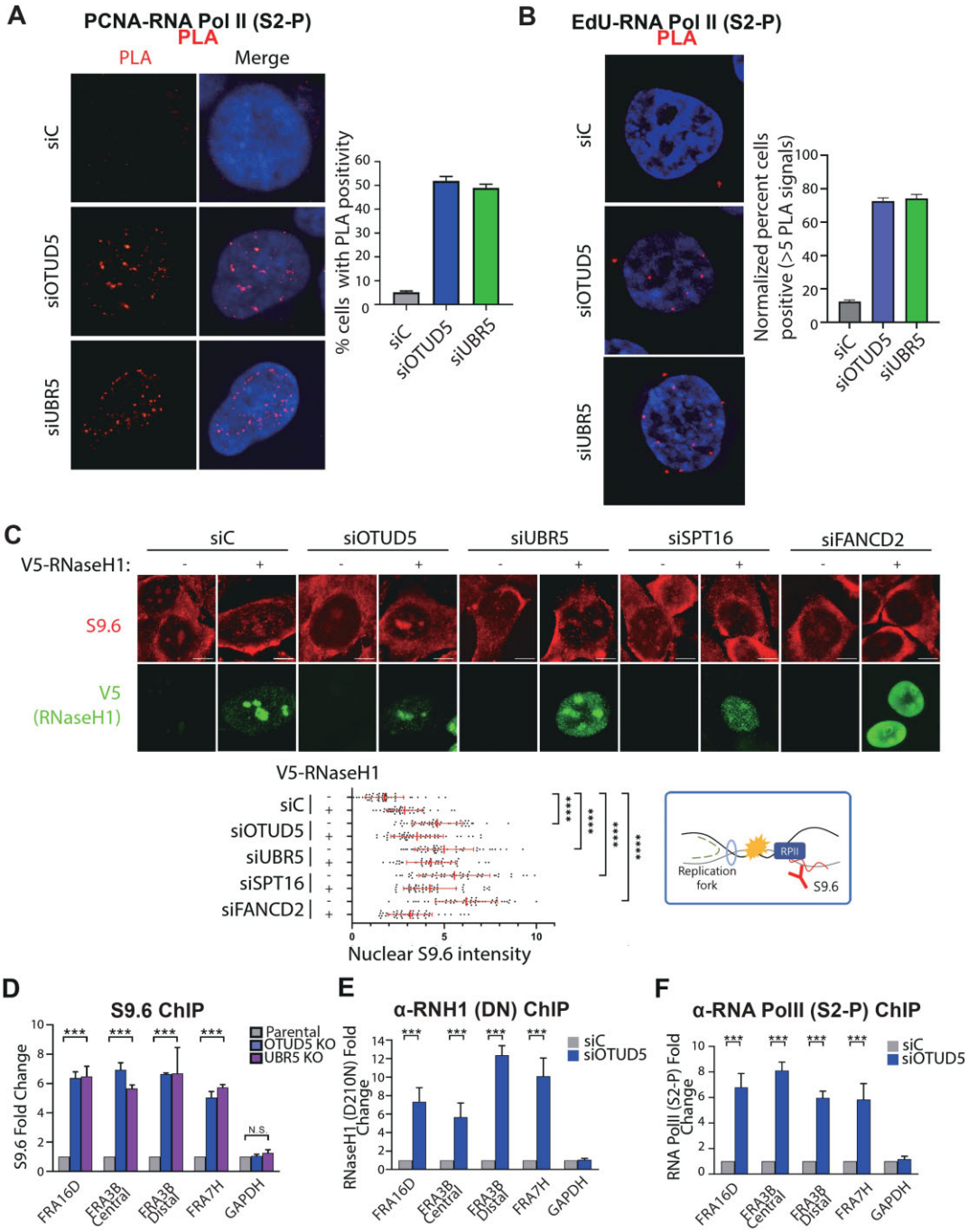

Figure 2. OTUD5 mitigates transcription-replication conflicts. (**A**) OTUD5 or UBR5 depletion causes increased proximity of PCNA and an elongating form of RNA polymerase II. Representative images of PCNA-RNA Pol II (S2-P) PLA in HeLa cells (left) transfected with indicated siRNAs, and quantification are shown (right). The experiment was conducted in triplicate (n = 50 in each experiment). (**B**) RNA Pol II (S2-P) is more present in nascent forks upon OTUD5 or UBR5 depletion. Representative images of PLA between EdU and RNA Pol II (S2-P) in HeLa cells transfected with indicated siRNAs (left). The percentage (normalized to biotin-biotin signals) of PLA signal positive cell is counted and plotted (right). The experiment was conducted in triplicate ($n = 50$ in each experiment). (**C**) DNA–RNA hybrids are increased in OTUD5 or UBR5-depleted cells. (Top) Representative images of S9.6 (red) and V5 immunostaining (green; for the V5-RNH1 transfected cells, S9.6 signals were quantified from V5-positive cells only). HeLa cells were transfected with indicated siRNAs. After 48 h, cells were transfected with V5-RNase H1 and then incubated for an additional 24 h. Cells were fixed and subjected to immunostaining. (Bottom) quantification of nuclear intensity of S9.6 staining ($n = 100$ for non-transfected control cells and $n = 60$ for V5 positive cells, $^{****}P < 0.0001$). (**D**) R-loops are significantly enriched in selected CFSs in OTUD5 or UBR5 knockout cells. ChIP using the S9.6 antibody followed by qPCR amplification with the indicated primers shows that R-loop level are increased at CFS in HeLa cells depleted of OTUD5 or UBR5, the experiment was conducted in triplicate ($^{***}P < 0.0005$). (**E**) Mutant RNH1 proteins are enriched in CFSs in OTUD5-depleted cells. qPCR quantification of RNaseH1 (D210N) ChIP in HeLa cells transfected with indicated siRNAs. Depleting OTUD5 increases catalytically inactive RNaseH1 fold enrichment at CFS, the experiment was conducted in triplicate ($^{***}P < 0.0005$). (**F**) RNAPII is increased at CFSs in OTUD5 knockdown cells. ChIP using the RNA Pol II (S2-P) antibody. HeLa cells were transfected with indicated siRNAs. Following qPCR amplification shows that elongating RNA pol II enriched at common fragile sites. The experiment was conducted in triplicate ($^{***}P < 0.0005$).

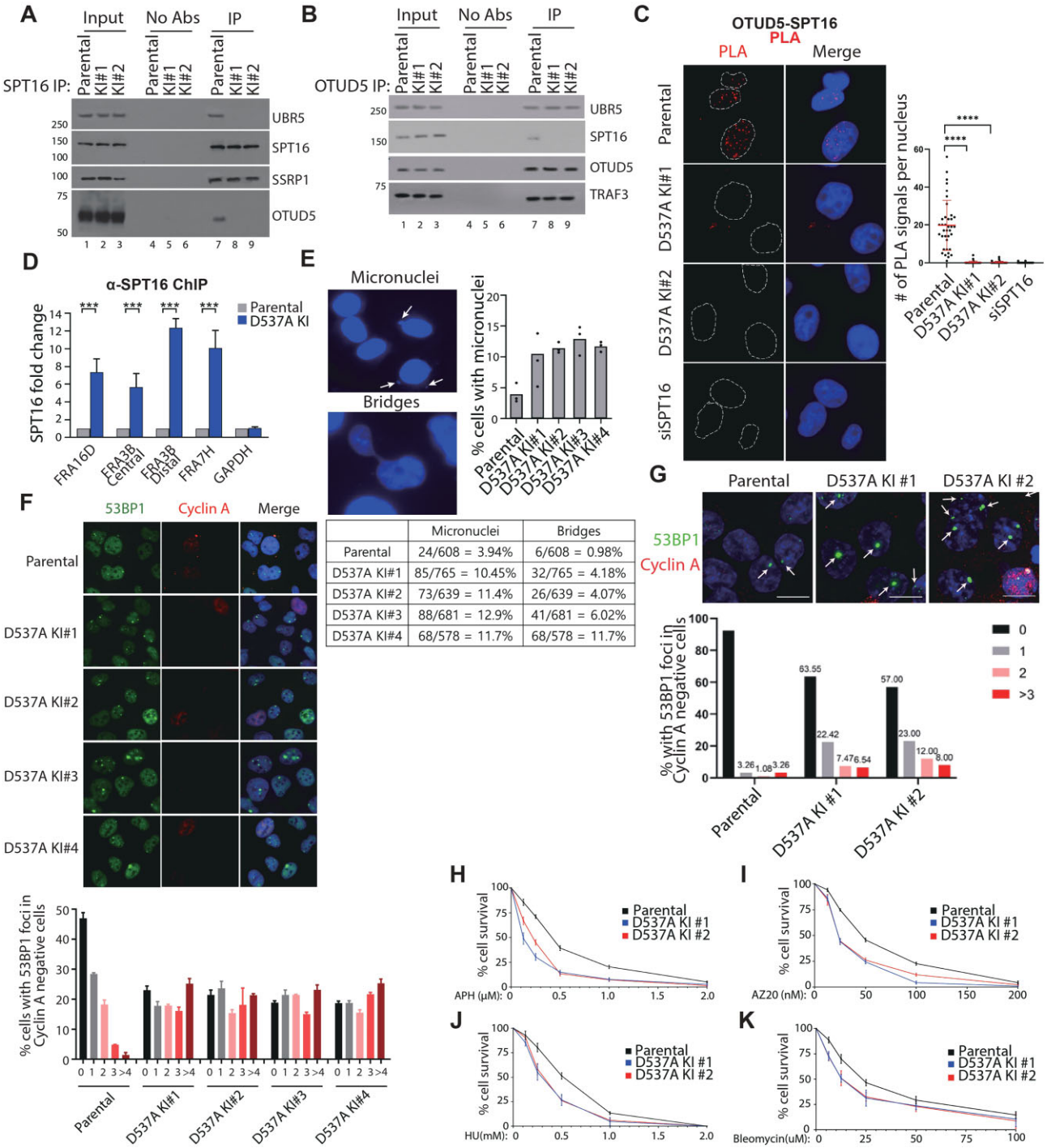

	Micronuclei	Bridges
Parental	24/608 = 3.94%	6/608 = 0.98%
D537A KI#1	85/765 = 10.45%	32/765 = 4.18%
D537A KI#2	73/639 = 11.4%	26/639 = 4.07%
D537A KI#3	88/681 = 12.9%	41/681 = 6.02%
D537A KI#4	68/578 = 11.7%	68/578 = 11.7%

Figure 3. Uncoupling the OTUD5-FACT complex leads replication stress. (**A**) FACT interaction with UBR5-OTUD5 proteins is lost in the *OTUD5*^{D537A} KI cells, as shown using α-SPT16 co-IP. Parental HeLa cell and *OTUD5*^{D537A} KI cells were harvested and lysed, and anti-SPT16 IP assay was performed. (**B**) The reverse co-IP using α-OTUD5 consistently finds similar results. Lysate from Parental HeLa cell and *OTUD5*^{D537A} KI cells were subject to anti-OTUD5 IP. (**C**) Disruption of the OTUD5-SPT16 interaction is confirmed using PLA in *OTUD5*^{D537A} KI cells. PLA (anti-OTUD5 + anti-SPT16 antibodies) was performed in HeLa cells. The number of PLA was counted and plotted using ImageJ ($n = 50$, $^{****}P > 0.0001$). (**D**) ChIP using the SPT16 antibody followed by qPCR amplification with indicated primers was performed. Enrichment of SPT16 at CFS increase in *OTUD5*^{D537A} KI cell, the experiment was conducted in triplicate ($^{***}P > 0.0005$). (**E**) The *OTUD5*^{D537A} KI cells display an increase in micronuclei (MN) and cytoplasmic bridges. Representative images of micronuclei and ultrafine bridges in *OTUD5*^{D537A} KI cell. Knock-in cell harboring D537A point mutation shows increased micronuclei and ultrafine bridges (left). Percentage of micronuclei is plotted (right). Cells were counted across three different experiments. (**F**) KI cells exhibit increased formation of 53BP1-NBs. (Top) Representative images of parental HeLa cell or *OTUD5*^{D537A} KI cells stained with 53BP1 and Cyclin A. (Buttom) Quantification of 53BP1 foci in Cyclin A negative cells ($n = 100$). (**G**) An increase of 53BP1-NBs is observed in HCT116 KI clones. (Top) Representative images of parental HCT116 cell or *OTUD5*^{D537A} KI cells stained with 53BP1 (green) and Cyclin A (red). 53BP1 nuclear body is indicated by arrows. (Bottom) Quantification of 53BP1 foci in Cyclin A negative cells ($n > 92$ in each case). (**H**–**K**) Parental HeLa cell and *OTUD5*^{D537A} KI cells were treated with indicated concentration of aphidicolin (APH), AZ20, hydroxyurea (HU) and bleomycin. Cells were incubated for 10 additional days, fixed, then stained using crystal violet.

undetectable in the nucleus of KI cells (Figure 3C). This finding was also confirmed in *OTUD5*^{D537A} KI clones generated in HCT116 cells (Supplementary Figure S4; sequencing information of two HCT116 clones is provided in Supplementary Figure S5).

To investigate how the uncoupling of FACT from OTUD5 affects FACT function, we performed anti-SPT16 ChIP to probe the occupation of SPT16 at selected CFS regions, and found SPT16 to be increased in the *OTUD5*^{D537A} cells (Figure 3D; IgG control is shown in Supplementary Figure S6). This result is consistent with our previous finding that FACT activity, as measured by the deposition rate of new histone H2A at DSBs, is increased in OTUD5-knockdown cells (37). Consistently, SPT16-EdU PLA increases in the KI cells (Supplementary Figure S7). Thus, blocking the interaction between FACT and OTUD5 enhances FACT nucleosome remodeling function.

The *OTUD5*^{D537A} cells display a noticeable increase in micronuclei and cytoplasmic bridges (Figure 3E), which can form as a consequence of replication stress. The frequency of MN formation is similar to that of OTUD5 or UBR5 knockdown cells (Figure 1D). Consistent with increased replication stress, the KI cells exhibited increased formation of 53BP1-NBs (Figure 3F). A similar increase of 53BP1-NBs was also observed in HCT116 KI clones (Figure 3G). We further found that the KI cells were sensitive to the DNA replication stress inducers aphidicolin, hydroxyurea, bleomycin (Figure 3H–K). The KI clones were also sensitive to the ATR inhibitor AZ20. Altogether, these results suggest that specific uncoupling of FACT from OTUD5 leads to DNA replication stress.

Uncoupling of FACT from OTUD5 leads to transcription-replication conflicts

We postulated that the increased replication stress in *OTUD5*^{D537A} KI cells could be caused by transcription-replication conflicts, based on the previous finding that FACT-mediated RNA Pol II activity is increased (or deregulated) at nuclease-induced DSBs when OTUD5 is depleted (37). Consistent with this notion, elongation of RNA Pol II is de-regulated at UVC-induced DNA breakage sites in the *OTUD5*^{D537A} clones (Supplementary Figure S8). Deregulated RNA Pol II activity can cause transcription stress and R-loop formations, resulting in DNA replication stress. We thus tested whether presence of elongating RNA Pol II (S2-P) is increased near nascent fork (marked by EdU) using a PLA. We found that, in four KI HCT116 clones, the EdU-RNA Pol II (S2-P) signal is drastically increased compared to wild type (Figure 4A). The PLA signals were also similarly increased in HeLa KI clones (Figure 4B, representative images are shown in Supplementary Figure S9). These results could suggest that either increased collisions taking place between the replisome and RNAPII (head-on), or increased (premature) transcription taking place that catches up behind the forks (co-directional). Aberrant accumulation of DNA–RNA hybrids is associated with transcription-replication conflicts (4). We tested whether R-loop formation is increased in CFSs in the KI clones, as CFSs are sites where TRCs are prone to occur (12). Indeed, we found an increased DNA–RNA hybrids (detected by the S9.6 antibody) at selected CFSs in a KI clone compared to wild type (Figure 4C). These results show that increased occupancy of FACT correlates with increased R-loops. Further, anti-S9.6 ChIP also showed that DNA–RNA hybrids are increased in these CFSs upon SPT16 knockdown (Figure 4D); this result is consistent with a previous study showing that FACT deficiency causes transcription-replication conflicts (35). Altogether, these results suggests that either too much or too little FACT activity can cause increase in DNA–RNA hybrid levels. The increased DNA–RNA hybrids could be a result of transcription stress, which can be reflected by increased presence of RNA Pol II at chromatin. Consistent with this notion, anti-RPB1 ChIP analysis showed increased RNA Pol II presence at CFSs in KI clones (Figure 4E). Imaging of nuclei with the S9.6 antibody showed that the S9.6 signal intensity is generally increased in the nucleoplasm area of KI clones, which are partially reduced by expressing wild type RNH1, suggesting that DNA–RNA hybrids are generally increased in KI cells (Figure 4F). R-loops can be eventually turned to DNA double strand breaks (43). We found that the levels of γH2AX foci are increased in the KI clones (Figure 4G), and interestingly, these foci are largely reduced back to control levels by expressing RNH1 (Figure 4H). These results suggest that increased DSBs formed in these KI clones mainly due to aberrant R-loop formations. Previous studies found that XPG nuclease mediates conversion of R-loops into DSBs (43,44). Consistent with these findings, depleting XPG significantly reduced γH2AX foci in KI clones (Figure 4I). Altogether, these results argue that uncoupling FACT from OTUD5 results in increased chromatin loading of FACT and transcription-replication conflicts.

To test if deregulation of FACT causes transcription-induced replication stress, we performed DNA fiber labeling analyses to measure replication fork speeds in *OTUD5*^{D537A} KI cells. Analysis of dually labelled replication tracts demonstrate that elongation rates are reduced in two independent *OTUD5*^{D537A} KI clones (Figure 4J). Since the KI cells exhibit increased R-loops and DSB induction, we analyzed fork symmetry using bidirectional replication forks. Heightened replication stress can collapse ongoing forks into DSBs that is revealed by an increased degree of replication fork asymmetry. Indeed, we find higher sister fork asymmetry in both KI clones compared to control cells (Figure 4K). Interestingly, the reduced replication fork was largely recovered by treating the cells with cordyceptin, an inhibitor of transcription (Figure 4L, M). These results argue that the reduced replication forks were largely due to interference by transcription activities.

OTUD5 regulates FACT activity by recruiting histone deacetylases

To gain mechanistic insights as to how OTUD5 limits FACT activity and R-loop formation, we turned our attention to study the FACT-associated proteins. To isolate proteins that associate with the FACT complex proteins, we introduced 3xFLAG into the N-terminus of *SPT16* loci in 293T cells using CRISPR Cas9 (Supplementary Figure S10; sequence info). Anti-FLAG immunoprecipitation followed by mass spectrometry identified HDAC1

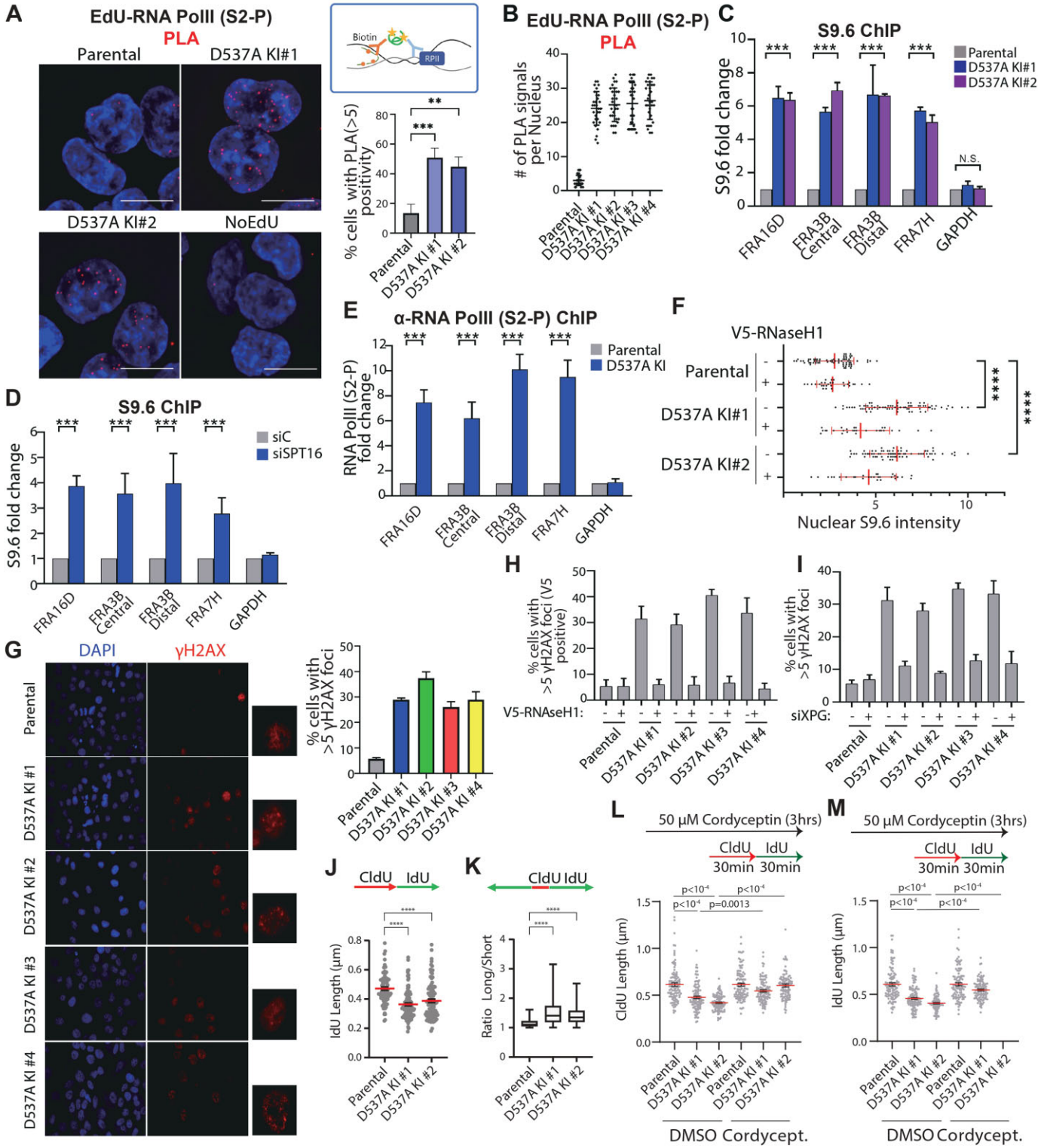

Figure 4. Uncoupling the OTUD5-FACT complex increases FACT loading and leads to transcription-induced genomic instability. (**A**) Uncoupling of FACT from OTUD5 increases elongating RNAPII in HCT116 cells. EdU-RNA Pol II (S2-P) PLA was performed in parental HCT116 cell and *OTUD5*^{D537A} KI cells. On the right is the quantification of percent of PLA signal numbering more than 5 with normalization to biotin-biotin. The experiment was performed in triplicate ($n = 75$). (**B**) Uncoupling of FACT from OTUD5 increases elongating RNAPII in HeLa cells. EdU-RNA Pol II (S2-P) PLA was performed in parental HeLa cells and *OTUD5*^{D537A} KI cells ($n = 100$, $^{****}P > 0.0001$). (**C**) Increased DNA–RNA hybrids occur at selected CFSs in a *OTUD5*^{D537A} KI cells as compared to wild type. qPCR quantification of S9.6 ChIP in parental HeLa cell or *OTUD5*^{D537A} KI HeLa cells ($^{***}P > 0.0005$). (**D**) DNA–RNA hybrids are increased in CFSs upon SPT16 knockdown. qPCR quantification of S9.6 ChIP in HeLa cell transfected with control or SPT16 siRNA ($^{***}P > 0.0005$). (**E**) Increased RNAPII presence occurs at CFSs in *OTUD5*^{D537A} KI clones. qPCR quantification of RNA Pol II (S2-P) ChIP in parental HeLa cell or *OTUD5*^{D537A} KI HeLa cell ($^{***}P > 0.0005$). (**F**) S9.6 signal intensity is increased in the nucleoplasm of KI clones,

and HDAC2 peptides, but not other HDAC members (Supplementary Figure S11). HDAC2 was a notable interactor, as OTUD5 also interacted with HDAC2 in a recent report (45). Western blot analysis of anti-FLAG-SPT16 IP confirmed the presence of HDAC1 and HDAC2 proteins in the eluate (Figure 5A). HDAC3 and HDAC4 were not detectable. Anti-FLAG-OTUD5 IP also co-precipitated HDAC1 and HDAC2, suggesting that OTUD5 also interacts with HDAC1 and HDAC2 (Figure 5B). Interestingly, the interaction between SPT16 and the HDAC proteins are indirectly mediated by OTUD5; while HDAC1 and HDAC2 proteins are found in SPT16 IP eluate from wild type cells, their presence is lost in *OTUD5*^{537A} cells, along with OTUD5 (Figure 5C). Anti-HDAC1 IP experiment consistently found that while SPT16 and SSRP1 are associated with HDAC1, their interactions are lost in *OTUD5*^{537A} cells (Figure 5D). Further, PLA detected the interaction between SPT16 and HDAC1 in wild type cells, but the signal is drastically lost in *OTUD5*^{537A} cells (Figure 5E), supporting the IP results. We previously identified the OTUD5 C-terminus disordered region to be required for interacting with FACT (37), but whether this region is sufficient was unknown. We thus extended this finding with bacterially purified GST-OTUD5 proteins; both full-length OTUD5 and a C-terminal fragment of OTUD5 (residues 501–571) similarly co-purified SPT16 (Figure 5F), suggesting that the C-terminus is sufficient to bind FACT. Interestingly, HDAC1 and HDAC2 are also able to interact with the C-terminal fragment of OTUD5. These results suggest that FACT and HDAC proteins are associated by tethering to the C-terminus of OTUD5.

One plausible hypothesis as to how OTUD5 regulates FACT activity is through recruiting HDAC1/2 and inducing histone deacetylation. Interestingly, a study found that in yeast, FACT proteins preferentially associate with acetylated histones (46). Although similar mechanism has not been reported in human cells, we postulate that human FACT proteins may be similarly regulated. First, we used PLA to test if the association between SPT16 and acetylated histone H4K16—which is known to occur at replication forks (47)—is detectable, and if so, if it is changed upon depleting HDAC1 and HDAC2. We found the SPT16/H4K16-ac PLA signals to be detectable and to be eliminated by knocking down SPT16 (Figure 5G). The PLA signals are increased upon co-depleting HDAC1 and HDAC2, or depleting OTUD5, albeit to a lower degree (Figure 5G), suggesting that the HDACs negatively regulate the association between SPT16 and the histones. The PLA signal is increased in two KI clones in comparison to parental cells (Figure 5H). This result is consistent with the finding that FACT enrichment in chromatin is increased in the KI cells (Figure 3D). ChIP assays further found that SPT16 occupancy at CFSs is increased in HDAC1 and HDAC2 knockdown cells, consistently suggesting that HDAC1 and HDAC2 negatively regulate the occupancy of FACT at these CFSs (Figure 5I). Furthermore, we found that HDAC1 and HDAC2 depletion increases R-loop formation, to a similar degree as SPT16 depletion (Figure 5J), consistent with the data that HDAC1/2 regulates FACT enrichment at chromatin.

While depleting OTUD5 does not affect the stability of FACT subunits, it decreased the stability of both HDAC1 and HDAC2, in cycloheximide-chase analysis (Supplementary Figure S12). This result suggests that OTUD5 promotes stability of the HDAC proteins. The stability of HDACs was partially rescued by a proteasome inhibitor MG132 (Figure 5K), and by re-expressing OTUD5 (Figure 5L). These results suggest that OTUD5 prevents the turnover of HDACs via ubiquitin-mediated proteasomal degradation. Altogether, these results suggest that the OTUD5-HDAC1/2 complex restricts aberrant FACT loading onto chromatin.

OTUD5^{D537A} cells require replication fork-protective proteins for survival

While the *OTUD5*^{D537A} clones exhibit increased replication fork stress and reduced ability to form colonies over time, they manage to survive for weeks in cultures. We reasoned that survival pathways (e.g. DNA repair) might be activated to help these cells to continue to proliferate. To unbiasedly interrogate factors or pathways that support the growth of these cells, we performed comparative phosphoproteomic analysis between wild type and the KI clones, focusing on SQ/TQ motifs, targets of ATM/ATR kinases (Figure 6A). Amongst many phosphorylations identified, phosphorylations of several Fanconi Anemia (FA) proteins were notable. The increase in phosphorylation of these sites in *OTUD5*^{D537A} KI clones was small (ranging from 1.1–1.4× times the phosphorylation levels in wild type cells), but the increase is consistent throughout the various sites in FA proteins. Indeed, foci formation of FANCD2, an indicator of FA pathway activation, is increased in the KI clones (Figure 6B). Interestingly, pre-treatment of fixed slides with RNH1 recombinant enzymes (per the method described in (39)) almost entirely eliminated the FANCD2 foci in the KI cells (Figure 6C), suggesting that the FANCD2 foci formed

←

which is partially reduced by expressing wild type RNH1. Nuclear S9.6 intensity with V5 positive in parental HCT116 cell or *OTUD5*^{D537A} KI cell. Cells were transfected with V5-RNaseH1, incubated for 24 h. Cells were fixed and treated with S9.6 antibody and α-V5 antibody ($n > 70$, $^{****}P > 0.0001$). (**G**) γH2AX foci are increased in the KI clones. (Left) Representative image of γH2AX immunostaining in parental HeLa cell or *OTUD5*^{D537A} KI HeLa cells. (Right) Quantification of percentage of cells with γH2AX foci numbering more than 5 is plotted ($n = 100$). (**H**) Foci are reduced by expressing RNH1. Quantification of percentage of cells with γH2AX foci numbering more than 5 is plotted ($n = 50$). Cells were transfected with or without V5-RNase H1 (for the V5-RNH1 transfected cells, S9.6 signals were quantified from V5-positive cells only). (**I**) Depleting XPG significantly reduces γH2AX foci in KI clones. Quantification of percentage of cells with γH2AX foci numbering more than 5 is plotted ($n = 50$). Cells were transfected with control or XPG siRNA. (**J**) Replication elongation is reduced in *OTUD5*^{D537A} KI HeLa cells. Parental HeLa and indicated OTUD5 KI clones were pulse labeled with CldU and IdU for 30 min each prior to DNA fiber analyses. IdU lengths were measured from dual labeled replication tracts and plotted. (**K**) IdU lengths were measured from bidirectional replication forks and ratios are plotted. *P* values were derived using Kruskal–Wallis one-way ANOVA corrected for multiple comparisons using Dunn's method with $P < 0.05$ as cutoff. 100 fibers were measured for figure J and at least 60 fibers were measured for figure K. (**L**–**M**) Treatment of transcription inhibitor cordyceptin rescues the elongation defect of *OTUD5*^{D537A} KI cells (L is for CldU and M is for IdU lengh).

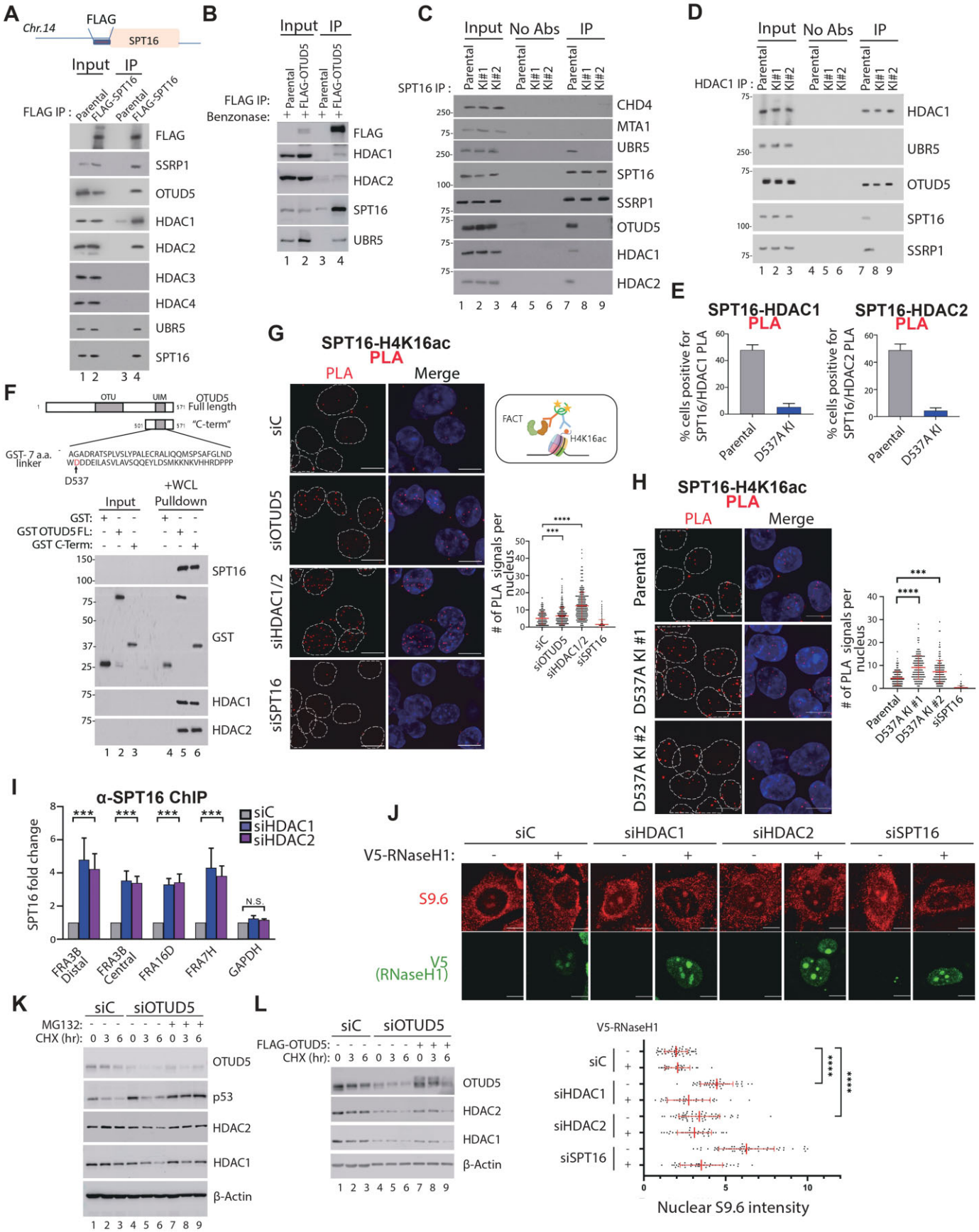

Figure 5. OTUD5-FACT complex mitigates replication stress through recruiting and stabilizing HDAC1 and HDAC2. (**A**) SPT16 specifically binds to HDAC1 and HDAC2. Parental 293T cells and FLAG-SPT16 CRISPR KI 293T cells were lysed and anti-FLAG IP was performed. (**B**) OTUD5

as a result of increased R-loop formation. FANCD2 foci were also increased when OTUD5 or UBR5 is depleted, which are reduced by overexpressing V5-tagged RNH1 (Figure 6D). As FA proteins are known to promote R-loop resolution, we reasoned that genomic instability of the *OTUD5^{D537A}* KI clones would be aggravated in the absence of FANCD2. Indeed, depleting FANCD2 increased γH2AX, more in KI cells as compared to wild type cells, suggesting that FA proteins prevent DSB formation in KI cells (Figure 6E). Depleting FANCD2 also reduced the viability of the KI cells as compared to parental cells, suggesting that the KI cells depend on the FA pathway for survival (Figure 6F).

DISCUSSION

Herein we report a new regulatory mechanism that limits transcription-replication conflicts. We found that OTUD5, and its binding partner UBR5, are modulators of transcription-induced replication fork stress. The role of OTUD5 in fork stress mitigation is pinpointed to its role in binding to and limiting the activity of the FACT histone chaperone. By utilizing cell lines engineered to uncouple FACT activity from OTUD5, we showed that increased FACT activity causes transcription-replication conflicts and R-loop formations. The FACT-limiting activity of OTUD5 is, at least in part, due to the recruitment and stabilization of the HDAC1 and HDAC2 proteins. Based on the data, we propose a model where the OTUD5-HDAC1-HDAC2 complex modulates FACT recruitment to nucleosomes by deacetylating them. In this model, OTUD5 traps FACT away from its target chromatin, keeping it in inactive state. Although our experimental evidence support that H4K16-Ac is a mark that mediates the FACT recruitment to chromatin, there may be other acetylation (e.g. H4K12-Ac, H4K5-Ac), which are also targets of HDACs, that could play roles in mediating the FACT recruitment. Based on the data, we propose a model where the OTUD5-HDAC1-HDAC2 complex modulates FACT recruitment to nucleosomes by deacetylating them (Figure 7). Interestingly, a recent report analyzing the proteome of R-loop modulators identified OTUD5, UBR5, HDAC1 and HDAC2 (48), consistent with our findings. This regulation may be particularly important in preserving stability of CFSs, where FACT activity is known to be enriched (49). Consistent with the roles of Fanconi Anemia proteins in CFS stability (50) and limiting aberrant R-loop formations (21,22), depletion of FANCD2 was synthetically lethal with loss of FACT regulation in the *OTUD5^{D537}* cells.

A previous study showed that depleting SPT16 increases DNA–RNA hybrids and genomic instability in yeast and human cells (35). DNA breaks accumulated in FACT-deficient cells were shown to be transcription-dependent, as overexpressing RNH1 largely rescued the genomic instability caused by FACT deficiency. Genomic instability phenotypes of the cell line with 'high-FACT' we described here were similarly rescued by RNH1 expression (Figures 2C, 4F, H, 5J, 6C and D). Importantly however, the de-regulated FACT activity did not cause an accelerated replication fork, but rather it caused the reverse (Figure 4J), unlike the case where high TOP1 expression led to lower R-loops and accelerated fork speed (51). Our results argue that too much FACT loading also causes aberrant R-loop accumulation and replication fork stress and emphasize that balancing the FACT activity is critical in mitigation of replication fork stress. Although we confined our studies to a few selected CFS regions, de-regulation of FACT may destabilize transcribed regions in a genome-wide fashion, particularly those containing long genes where the chances of transcription-replication conflict are higher. We also propose that the high-FACT situation we describe mimics cancer cells with high FACT activity (52). Therefore, it is possible that such high-FACT cancers may also experience high levels of replication stress and R-loops, and depend on genome-stabilizing factors for survival. Further studies may enlighten the cryptic regulations that support the survival of FACT-driven cancers.

HDAC1 and HDAC2 belong to the class I of histone deacetylases (HDACs) that are ubiquitously expressed in most mammalian cells (53). Genetic knockdown or pharmacological inactivation of HDAC1 and HDAC2 attenuates cell growth and induces cell death (54) – this could be, at least in part, due to increased replication stress, as depleting HDAC1 or HDAC2 was shown to cause replication stress (47). Consistently, HDAC1 and HDAC2 were identified to be components of nascent fork proteome (55),

←

interacts with HDAC1 and HDAC2. 293T cells and stably expressing FLAG-OTUD5 cells were lysed, and anti-FLAG IP was performed with 250U benzonase treatment. (**C**) HDAC1 and HDAC2 proteins do not interact with SPT16 in *OTUD5^{537A}* cells. Co-IP using anti-SPT16 antibody was performed in parental HeLa cells and *OTUD5^{D537A}* KI cells. (**D**) SPT16 and SSRP1 interactions with HDAC1 are lost in *OTUD5^{537A}* cells. Co-IP using anti-HDAC1 was performed in parental HeLa cells and *OTUD5^{D537A}* KI cells. (**E**) SPT16 and HDAC1 or HDAC2 interact in wild type cells but not in *OTUD5^{537A}* cells. PLA (anti-HDAC1 or anti-HDAC2 + anti-SPT16 antibodies) was performed in HeLa cells. The experiment was conducted in triplicate. The percentage of cells with PLA positive is counted and plotted using ImageJ ($n = 100$ in each experiment). (**F**) The C-terminus of OTUD5 is sufficient to bind FACT. (Top) Schematic of full length OTUD5 a C-terminal truncation. The GST tag is on the N-terminus. (Bottom) GST pulldown, bacterial expression of GST-OTUD5 were purified using glutathione beads. The beads were applied to whole cell lysate (WCL) of 293T cells for pulldown. (**G**) SPT16/H4K16-ac PLA signals are eliminated by knocking down SPT16. PLA (α-SPT16 + α-H4K16ac) was performed in HCT116 cell. Cells were transfected with indicated siRNAs and incubated for 72 h. Cells were fixed and used for PLA. Representative images (left) and its quantification (right) ($n = 256$, $^{***}P > 0.0005$, $^{****}P > 0.0001$). (**H**) The SPT16/H4K16-ac PLA signal is increased in KI clones. PLA (α-SPT16 + α-H4K16ac) was performed in parental HCT116 and *OTUD5^{D537A}* KI cells ($n > 140$, $^{****}P > 0.0001$). (**I**) SPT16 occupancy at CFSs is increased in HDAC1 and HDAC2 knockdown cells. qPCR quantification of SPT16 ChIP in HeLa cells transfected with control or indicated siRNAs ($^{***}P > 0.0005$). Cells were incubated for 72 h followed by transfection, then fixed and subjected to ChIP, the experiment was conducted in triplicate. (**J**) HDAC1 and HDAC2 depletion increases R-loop formation. Representative images (left) and its quantification (right). siRNAs were transfected into HCT116 cells and stained with S9.6 antibody (For the V5-RNH1 transfected cells, S9.6 signals were quantified from V5-positive cells only) ($n > 70$, $^{****}P > 0.0001$). (**K**) The stability of HDACs can be rescued by the proteasome inhibitor MG132. Cycloheximide chase experiment was performed in cells transfected with siOTUD5, followed by cycloheximide treatment (25 μM, for the indicated h) and followed by MG132 treatment (10 μM for indicated time points). (**L**) The stability of HDACs can be rescued by re-expressing wild type OTUD5. Cycloheximide chase experiment was performed using HCT116 cells with transfection of indicated siRNA and plasmid.

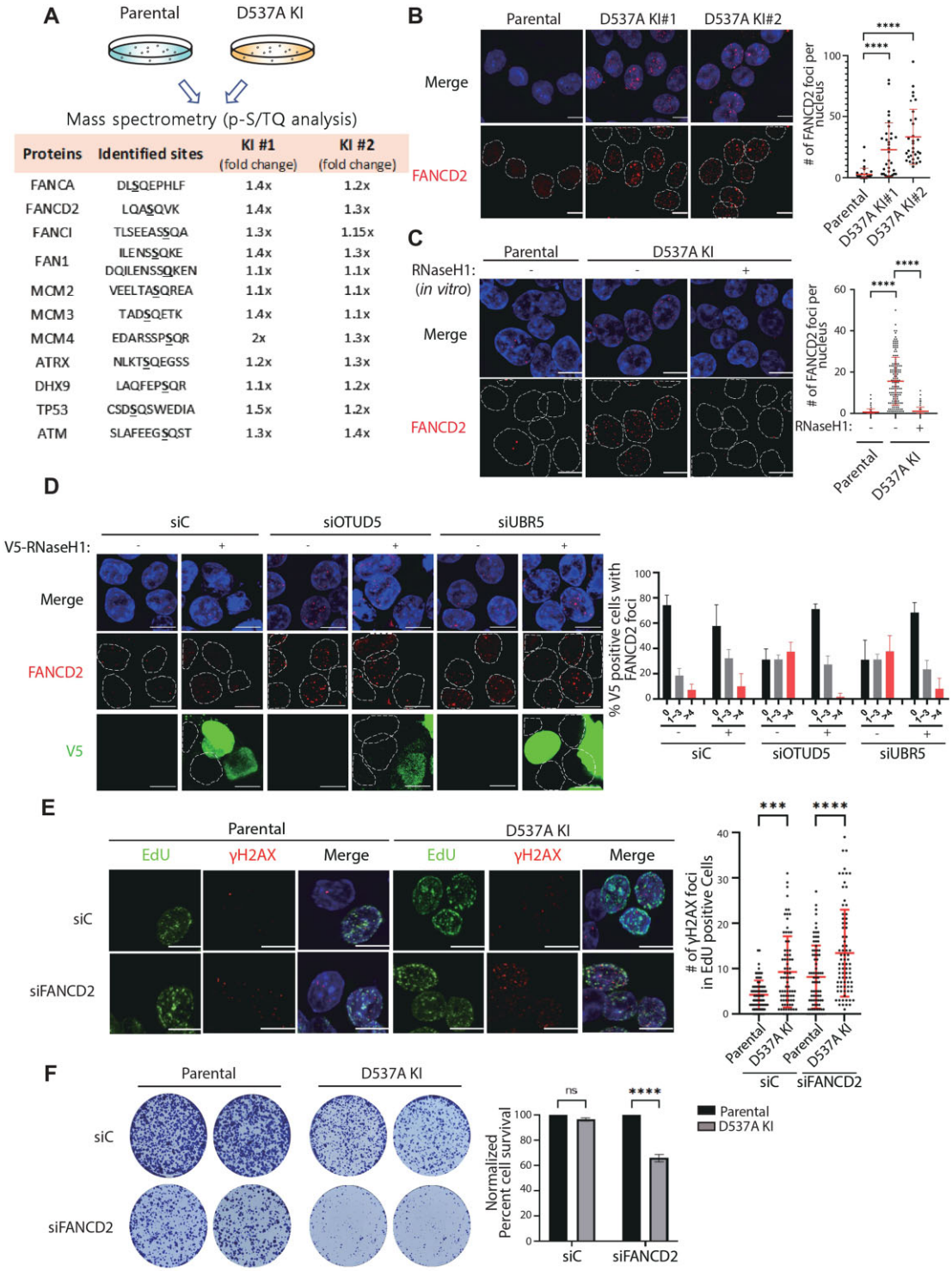

Proteins	Identified sites	KI #1 (fold change)	KI #2 (fold change)
FANCA	DLSQEPHLF	1.4x	1.2x
FANCD2	LQASQVK	1.4x	1.3x
FANCI	TLSEEASSQA	1.3x	1.15x
FAN1	ILENSSQKE	1.4x	1.3x
	DQILENSSQKEN	1.1x	1.1x
MCM2	VEELTASQREA	1.1x	1.1x
MCM3	TADSQETK	1.4x	1.1x
MCM4	EDARSSPSQR	2x	1.3x
ATRX	NLKTSQEGSS	1.2x	1.3x
DHX9	LAQFEPSQR	1.1x	1.2x
TP53	CSDSQSWEDIA	1.5x	1.2x
ATM	SLAFEEGSQST	1.3x	1.4x

Figure 6. Fanconi Anemia proteins mitigate R-loop stress induced in *OTUD5*^{D537A} KI cells. (**A**) Schematic for phospho-site mass spectrometry. Parental HeLa cells and two clones of *OTUD5*^{D537A} CRISPR KI cells were harvested and extracted peptides were subject to ion chromatograms for relative quantitation with Skyline software. (**B**) FANCD2 foci are increased in the KI clones. Representative images of FANCD2 foci (left) in parental HCT116 and *OTUD5*^{D537A} KI HCT116 cell and its quantification (right) ($n = 32$). Cells were seeded on 12-well plates and immunofluorescence were performed after 24 h. (**C**) RNH1 eliminates FANCD2 foci in the KI cells. Representative images of FANCD2 foci (left) in parental HCT116 and *OTUD5*^{D537A} KI HCT116 cells are shown (quantification in right; $n = 145$ each; see methods). (**D**) FANCD2 foci are increased when OTUD5 or UBR5 is depleted. Representative images of FANCD2 foci (top). HCT116 Cells were transfected with indicated siRNAs then incubated for 48 h. Cells were additionally incubated for 24 h after transfection of V5-RNase H1. Quantification of FANCD2 foci in V5-positive cell (bottom) ($n > 38$). (**E**) FANCD2 prevents DSB formation in KI cells. Representative images show EdU and γH2AX foci in parental and *OTUD5*^{D537A} KI cells. Each cell line was transfected with siFANCD2. Graph shows quantification of γH2AX foci in EdU positive cells ($n = 80$, $^{***}P < 0.0005$, $^{****}P < 0.00001$). (**F**) Clonogenic assay shows that viability of *OTUD5*^{D537A} KI cells is reduced by depletion of FANCD2.

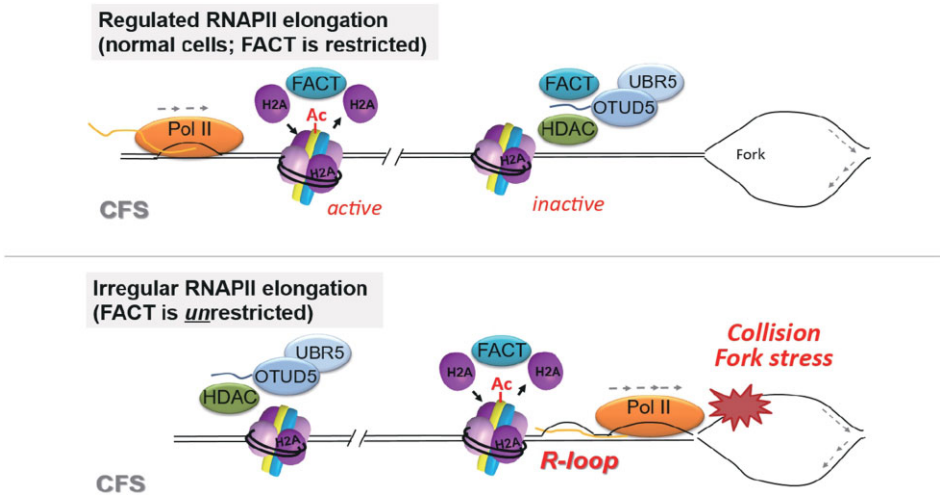

Figure 7. Model. (Top) FACT-driven RNAPII elongation is regulated by OTUD5-HDAC1/2. HDAC1/2-mediated deacetylation of nucleosomes reduces FACT recruitment and local transcription. (Bottom) Inactivation (or deficiency) of OTUD5 or HDAC1/2 causes FACT to be deregulated, leading to transcription stress and replication fork collisions.

which emphasizes the role of HDACs in preserving replication fork integrity. HDAC1 and HDAC2 were also identified as regulators of DSB-induced transcription silencing (56), similar to OTUD5 and UBR5 (37,57). How HDAC1 and HDAC2 are regulated or spatially organized at the stressed replication fork has not been well understood. To our knowledge, our study, for the first time, has found that HDAC1 and HDAC2 form a complex with the histone chaperone FACT. HDAC1 and HDAC2 can be integral parts of multi-subunit gene-repressive complexes, such as Sin3, NuRD (nucleosome remodeling and deacetylation), or CoREST (co-repressor for element-1-silencing transcription factor), to regulate local histone acetylation and transcriptional repression under various physiological contexts (53). By forming a complex with FACT and OTUD5, the HDAC proteins may serve a specialized function at replication forks to limit conflicts with transcription machineries. Further biochemical studies will enlighten the precise architecture of this complex. Our work also suggests that FACT recruitment to nucleosomes in human cells may be enhanced by histone acetylation, as it is in yeast (46). Our work also identifies OTUD5 as a potential deubiquitinase and stabilizer for HDAC1 and HDAC2. It is possible that OTUD5's role in regulating replication stress or TRC could be broader than suggested herein, as OTUD5 is known to regulate other chromatin remodelers such as ARID1A (45).

Several factors have been shown to limit aberrant R-loop accumulations. These include helicases such as SENATAXIN (58), DHX9 (20,59), DDX47 (60), UAP56/DDX39B (61), or Fanconi Anemia proteins (17,21–23,62,63). FANCD2, a central platform protein in the FA pathway, is increasingly appreciated in its role for resolving R-loops. FANCD2 was suggested to recruit several proteins that help resolve R-loops, including FANCM and RNA processing factors (21,63). MRN (MRE11-RAD50-NBS1) complex was also shown to act in a linear pathway with FANCD2 in limiting R-loop formation (62). Depleting FANCD2 in the *OTUD5*^{D537A} background led to synergistic increase in DSB formation and cell death (Figure 6F), consistent with the role of these proteins in limiting R-loops. We previously showed that depleting FANCD2 also caused synthetic lethality in RNF2-deficient cells (12). This study also showed that R-loops were increased at replication forks in the absence of the epigenetic silencers RNF2 or BMI1, leading to fork stress and transcription-replication collision. These results suggest that FA proteins act as universal factors that promote recovery of stressed replication induced by R-loops. We also speculate that cancers that have overexpressed FACT may experience increased transcription-induced conflicts and R-loop formation and that these cancers may depend on the FA proteins for survival. Our finding may also provide a new therapeutic avenue for cancer. Disrupting the disorder-mediated interactions amongst the OTUD5, FACT and HDAC proteins may represent a strategy to enhance R-loop stress in cancer cells, particularly those deficient in the FA pathway. In summary, our work identifies a new mode of regulation that limits transcription and replication conflicts and preserves genomic integrity.

DATA AVAILABILITY

The datasets generated during and/or analysed during the current study are available from the corresponding authors on reasonable request.

SUPPLEMENTARY DATA

Supplementary Data are available at NAR Online.

ACKNOWLEDGEMENTS

We thank the WASHU Genome Engineering & iPSC center for generating all CRISPR cell lines, and Dr Bin Fang at the Proteomics and Metabolomics Core at the H.Lee Moffitt Cancer Center & Research Institute for proteomic analysis. pyCAG_RNaseH1_WT and D210N plasmids were gifts

from Dr Xiang-Dong Fu through Addgene. We thank the members of the Kee laboratory for critical review of the manuscripts.

FUNDING

National Institutes of Health [R01GM117062-01A1]; National Research Foundation of Korea [NRF-2021R1A2C1093818 to Y.K.]; Moffitt's Cancer Center Support Grant [P30-CA076292]. Funding for open access charge: [R01GM117062-01A1].
Conflict of interest statement. None declared.

REFERENCES

1. Kim,N. and Jinks-Robertson,S. (2012) Transcription as a source of genome instability. *Nat. Rev. Genet.*, **13**, 204–214.
2. Sarni,D. and Kerem,B. (2016) The complex nature of fragile site plasticity and its importance in cancer. *Curr. Opin. Cell Biol.*, **40**, 131–136.
3. Santos-Pereira,J.M. and Aguilera,A. (2015) R loops: new modulators of genome dynamics and function. *Nat. Rev. Genet.*, **16**, 583–597.
4. Hamperl,S., Bocek,M.J., Saldivar,J.C., Swigut,T. and Cimprich,K.A. (2017) Transcription-replication conflict orientation modulates R-loop levels and activates distinct DNA damage responses. *Cell*, **170**, 774–786.
5. Urban,V., Dobrovolna,J., Huhn,D., Fryzelkova,J., Bartek,J. and Janscak,P. (2016) RECQ5 helicase promotes resolution of conflicts between replication and transcription in human cells. *J. Cell Biol.*, **214**, 401–415.
6. Tuduri,S., Crabbe,L., Conti,C., Tourriere,H., Holtgreve-Grez,H., Jauch,A., Pantesco,V., De Vos,J., Thomas,A., Theillet,C. *et al.* (2009) Topoisomerase I suppresses genomic instability by preventing interference between replication and transcription. *Nat. Cell Biol.*, **11**, 1315–1324.
7. Liu,Y., Lin,Y.L., Pasero,P. and Chen,C.L. (2020) Topoisomerase I prevents transcription-replication conflicts at transcription termination sites. *Mol Cell Oncol*, **8**, 1843951.
8. Promonet,A., Padioleau,I., Liu,Y., Sanz,L., Biernacka,A., Schmitz,A.L., Skrzypczak,M., Sarrazin,A., Mettling,C., Rowicka,M. *et al.* (2020) Topoisomerase 1 prevents replication stress at R-loop-enriched transcription termination sites. *Nat. Commun.*, **11**, 3940.
9. Salas-Armenteros,I., Perez-Calero,C., Bayona-Feliu,A., Tumini,E., Luna,R. and Aguilera,A. (2017) Human THO-Sin3A interaction reveals new mechanisms to prevent R-loops that cause genome instability. *EMBO J.*, **36**, 3532–3547.
10. Bayona-Feliu,A., Barroso,S., Munoz,S. and Aguilera,A. (2021) The SWI/SNF chromatin remodeling complex helps resolve R-loop-mediated transcription-replication conflicts. *Nat. Genet.*, **53**, 1050–1063.
11. Prendergast,L., McClurg,U.L., Hristova,R., Berlinguer-Palmini,R., Greener,S., Veitch,K., Hernandez,I., Pasero,P., Rico,D., Higgins,J.M.G. *et al.* (2020) Resolution of R-loops by INO80 promotes DNA replication and maintains cancer cell proliferation and viability. *Nat. Commun.*, **11**, 4534.
12. Sanchez,A., de Vivo,A., Tonzi,P., Kim,J., Huang,T.T. and Kee,Y. (2020) Transcription-replication conflicts as a source of common fragile site instability caused by BMI1-RNF2 deficiency. *PLoS Genet.*, **16**, e1008524.
13. Chen,L., Chen,J.Y., Huang,Y.J., Gu,Y., Qiu,J., Qian,H., Shao,C., Zhang,X., Hu,J., Li,H. *et al.* (2018) The augmented R-loop is a unifying mechanism for myelodysplastic syndromes induced by high-risk splicing factor mutations. *Mol. Cell*, **69**, 412–425.
14. Arif,W., Mathur,B., Saikali,M.F., Chembazhi,U.V., Toohill,K., Song,Y.J., Hao,Q., Karimi,S., Blue,S.M., Yee,B.A. *et al.* (2023) Splicing factor SRSF1 deficiency in the liver triggers NASH-like pathology and cell death. *Nat. Commun.*, **14**, 551.
15. Jimenez,M., Urtasun,R., Elizalde,M., Azkona,M., Latasa,M.U., Uriarte,I., Arechederra,M., Alignani,D., Barcena-Varela,M., Alvarez-Sola,G. *et al.* (2019) Splicing events in the control of genome integrity: role of SLU7 and truncated SRSF3 proteins. *Nucleic Acids Res.*, **47**, 3450–3466.
16. Wu,W., Bhowmick,R., Vogel,I., Ozer,O., Ghisays,F., Thakur,R.S., Sanchez de Leon,E., Richter,P.H., Ren,L., Petrini,J.H. *et al.* (2020) RTEL1 suppresses G-quadruplex-associated R-loops at difficult-to-replicate loci in the human genome. *Nat. Struct. Mol. Biol.*, **27**, 424–437.
17. Takedachi,A., Despras,E., Scaglione,S., Guerois,R., Guervilly,J.H., Blin,M., Audebert,S., Camoin,L., Hasanova,Z., Schertzer,M. *et al.* (2020) SLX4 interacts with RTEL1 to prevent transcription-mediated DNA replication perturbations. *Nat. Struct. Mol. Biol.*, **27**, 438–449.
18. Lam,F.C., Kong,Y.W., Huang,Q., Vu Han,T.L., Maffa,A.D., Kasper,E.M. and Yaffe,M.B. (2020) BRD4 prevents the accumulation of R-loops and protects against transcription-replication collision events and DNA damage. *Nat. Commun.*, **11**, 4083.
19. Li,M., Xu,X., Chang,C.W., Zheng,L., Shen,B. and Liu,Y. (2018) SUMO2 conjugation of PCNA facilitates chromatin remodeling to resolve transcription-replication conflicts. *Nat. Commun.*, **9**, 2706.
20. Kim,S., Kang,N., Park,S.H., Wells,J., Hwang,T., Ryu,E., Kim,B.G., Hwang,S., Kim,S.J., Kang,S. *et al.* (2020) ATAD5 restricts R-loop formation through PCNA unloading and RNA helicase maintenance at the replication fork. *Nucleic Acids Res.*, **48**, 7218–7238.
21. Schwab,R.A., Nieminuszczy,J., Shah,F., Langton,J., Lopez Martinez,D., Liang,C.C., Cohn,M.A., Gibbons,R.J., Deans,A.J. and Niedzwiedz,W. (2015) The fanconi anemia pathway maintains genome stability by coordinating replication and transcription. *Mol. Cell*, **60**, 351–361.
22. Garcia-Rubio,M.L., Perez-Calero,C., Barroso,S.I., Tumini,E., Herrera-Moyano,E., Rosado,I.V. and Aguilera,A. (2015) The Fanconi anemia pathway protects genome integrity from R-loops. *PLoS Genet.*, **11**, e1005674.
23. Liang,Z., Liang,F., Teng,Y., Chen,X., Liu,J., Longerich,S., Rao,T., Green,A.M., Collins,N.B., Xiong,Y. *et al.* (2019) Binding of FANCI-FANCD2 complex to RNA and R-loops stimulates robust FANCD2 monoubiquitination. *Cell Rep.*, **26**, 564–572.
24. Pan,X., Chen,Y., Biju,B., Ahmed,N., Kong,J., Goldenberg,M., Huang,J., Mohan,N., Klosek,S., Parsa,K. *et al.* (2019) FANCM suppresses DNA replication stress at ALT telomeres by disrupting TERRA R-loops. *Sci. Rep.*, **9**, 19110.
25. Hodson,C., van Twest,S., Dylewska,M., O'Rourke,J.J., Tan,W., Murphy,V.J., Walia,M., Abbouche,L., Nieminuszczy,J., Dunn,E. *et al.* (2022) Branchpoint translocation by fork remodelers as a general mechanism of R-loop removal. *Cell Rep.*, **41**, 111749.
26. Shao,X., Joergensen,A.M., Howlett,N.G., Lisby,M. and Oestergaard,V.H. (2020) A distinct role for recombination repair factors in an early cellular response to transcription-replication conflicts. *Nucleic Acids Res.*, **48**, 5467–5484.
27. Bhatia,V., Barroso,S.I., Garcia-Rubio,M.L., Tumini,E., Herrera-Moyano,E. and Aguilera,A. (2014) BRCA2 prevents R-loop accumulation and associates with TREX-2 mRNA export factor PCID2. *Nature*, **511**, 362–365.
28. Wang,Y., Ma,B., Liu,X., Gao,G., Che,Z., Fan,M., Meng,S., Zhao,X., Sugimura,R., Cao,H. *et al.* (2022) ZFP281-BRCA2 prevents R-loop accumulation during DNA replication. *Nat. Commun.*, **13**, 3493.
29. Shivji,M.K.K., Renaudin,X., Williams,C.H. and Venkitaraman,A.R. (2018) BRCA2 regulates transcription elongation by RNA polymerase II to prevent R-loop accumulation. *Cell Rep.*, **22**, 1031–1039.
30. Sessa,G., Gomez-Gonzalez,B., Silva,S., Perez-Calero,C., Beaurepere,R., Barroso,S., Martineau,S., Martin,C., Ehlen,A., Martinez,J.S. *et al.* (2021) BRCA2 promotes DNA–RNA hybrid resolution by DDX5 helicase at DNA breaks to facilitate their repairdouble dagger. *EMBO J.*, **40**, e106018.
31. D'Alessandro,G., Whelan,D.R., Howard,S.M., Vitelli,V., Renaudin,X., Adamowicz,M., Iannelli,F., Jones-Weinert,C.W., Lee,M., Matti,V. *et al.* (2018) BRCA2 controls DNA:RNA hybrid level at DSBs by mediating RNase H2 recruitment. *Nat. Commun.*, **9**, 5376.
32. Hatchi,E., Skourti-Stathaki,K., Ventz,S., Pinello,L., Yen,A., Kamieniarz-Gdula,K., Dimitrov,S., Pathania,S., McKinney,K.M., Eaton,M.L. *et al.* (2015) BRCA1 recruitment to transcriptional pause sites is required for R-loop-driven DNA damage repair. *Mol. Cell*, **57**, 636–647.

33. Zhang,X., Chiang,H.C., Wang,Y., Zhang,C., Smith,S., Zhao,X., Nair,S.J., Michalek,J., Jatoi,I., Lautner,M. *et al.* (2017) Attenuation of RNA polymerase II pausing mitigates BRCA1-associated R-loop accumulation and tumorigenesis. *Nat. Commun.*, **8**, 15908.
34. Makharashvili,N., Arora,S., Yin,Y., Fu,Q., Wen,X., Lee,J.H., Kao,C.H., Leung,J.W., Miller,K.M. and Paull,T.T. (2018) Sae2/CtIP prevents R-loop accumulation in eukaryotic cells. *eLife*, **7**, e42733.
35. Herrera-Moyano,E., Mergui,X., Garcia-Rubio,M.L., Barroso,S. and Aguilera,A. (2014) The yeast and human FACT chromatin-reorganizing complexes solve R-loop-mediated transcription-replication conflicts. *Genes Dev.*, **28**, 735–748.
36. Gurova,K., Chang,H.W., Valieva,M.E., Sandlesh,P. and Studitsky,V.M. (2018) Structure and function of the histone chaperone FACT - Resolving FACTual issues. *Biochim. Biophys. Acta Gene Regul. Mech.*, **1861**, 892–904.
37. de Vivo,A., Sanchez,A., Yegres,J., Kim,J., Emly,S. and Kee,Y. (2019) The OTUD5-UBR5 complex regulates FACT-mediated transcription at damaged chromatin. *Nucleic Acids Res.*, **47**, 729–746.
38. Lukas,C., Savic,V., Bekker-Jensen,S., Doil,C., Neumann,B., Pedersen,R.S., Grofte,M., Chan,K.L., Hickson,I.D., Bartek,J. *et al.* (2011) 53BP1 nuclear bodies form around DNA lesions generated by mitotic transmission of chromosomes under replication stress. *Nat. Cell Biol.*, **13**, 243–253.
39. Crossley,M.P., Brickner,J.R., Song,C., Zar,S.M.T., Maw,S.S., Chedin,F., Tsai,M.S. and Cimprich,K.A. (2021) Catalytically inactive, purified RNase H1: a specific and sensitive probe for RNA–DNA hybrid imaging. *J. Cell Biol.*, **220**, e202101092.
40. Parajuli,S., Teasley,D.C., Murali,B., Jackson,J., Vindigni,A. and Stewart,S.A. (2017) Human ribonuclease H1 resolves R-loops and thereby enables progression of the DNA replication fork. *J. Biol. Chem.*, **292**, 15216–15224.
41. Paulsen,R.D., Soni,D.V., Wollman,R., Hahn,A.T., Yee,M.C., Guan,A., Hesley,J.A., Miller,S.C., Cromwell,E.F., Solow-Cordero,D.E. *et al.* (2009) A genome-wide siRNA screen reveals diverse cellular processes and pathways that mediate genome stability. *Mol. Cell*, **35**, 228–239.
42. Saponaro,M., Kantidakis,T., Mitter,R., Kelly,G.P., Heron,M., Williams,H., Soding,J., Stewart,A. and Svejstrup,J.Q. (2014) RECQL5 controls transcript elongation and suppresses genome instability associated with transcription stress. *Cell*, **157**, 1037–1049.
43. Sollier,J., Stork,C.T., Garcia-Rubio,M.L., Paulsen,R.D., Aguilera,A. and Cimprich,K.A. (2014) Transcription-coupled nucleotide excision repair factors promote R-loop-induced genome instability. *Mol. Cell*, **56**, 777–785.
44. Cristini,A., Ricci,G., Britton,S., Salimbeni,S., Huang,S.N., Marinello,J., Calsou,P., Pommier,Y., Favre,G., Capranico,G. *et al.* (2019) Dual processing of R-loops and topoisomerase I induces transcription-dependent DNA double-strand breaks. *Cell Rep.*, **28**, 3167–3181.
45. Beck,D.B., Basar,M.A., Asmar,A.J., Thompson,J.J., Oda,H., Uehara,D.T., Saida,K., Pajusalu,S., Talvik,I., D'Souza,P. *et al.* (2021) Linkage-specific deubiquitylation by OTUD5 defines an embryonic pathway intolerant to genomic variation. *Sci. Adv.*, **7**, eabe2116.
46. Pathak,R., Singh,P., Ananthakrishnan,S., Adamczyk,S., Schimmel,O. and Govind,C.K. (2018) Acetylation-dependent recruitment of the FACT complex and its role in regulating Pol II occupancy genome-wide in *Saccharomyces cerevisiae*. *Genetics*, **209**, 743–756.
47. Bhaskara,S., Jacques,V., Rusche,J.R., Olson,E.N., Cairns,B.R. and Chandrasekharan,M.B. (2013) Histone deacetylases 1 and 2 maintain S-phase chromatin and DNA replication fork progression. *Epigenetics Chromatin*, **6**, 27.
48. Yan,Q., Wulfridge,P., Doherty,J., Fernandez-Luna,J.L., Real,P.J., Tang,H.Y. and Sarma,K. (2022) Proximity labeling identifies a repertoire of site-specific R-loop modulators. *Nat. Commun.*, **13**, 53.
49. Kim,J., Sturgill,D., Sebastian,R., Khurana,S., Tran,A.D., Edwards,G.B., Kruswick,A., Burkett,S., Hosogane,E.K., Hannon,W.W. *et al.* (2018) Replication stress shapes a protective chromatin environment across fragile genomic regions. *Mol. Cell*, **69**, 36–47.
50. Okamoto,Y., Iwasaki,W.M., Kugou,K., Takahashi,K.K., Oda,A., Sato,K., Kobayashi,W., Kawai,H., Sakasai,R., Takaori-Kondo,A. *et al.* (2018) Replication stress induces accumulation of FANCD2 at central region of large fragile genes. *Nucleic Acids Res.*, **46**, 2932–2944.
51. Sarni,D., Barroso,S., Shtrikman,A., Irony-Tur Sinai,M., Oren,Y.S., Aguilera,A and Kerem,B. (2022) Topoisomerase 1-dependent R-loop deficiency drives accelerated replication and genomic instability. *Cell Rep.*, **40**, 111397.
52. Garcia,H., Miecznikowski,J.C., Safina,A., Commane,M., Ruusulehto,A., Kilpinen,S., Leach,R.W., Attwood,K., Li,Y., Degan,S. *et al.* (2013) Facilitates chromatin transcription complex is an "accelerator" of tumor transformation and potential marker and target of aggressive cancers. *Cell Rep.*, **4**, 159–173.
53. Kelly,R.D. and Cowley,S.M. (2013) The physiological roles of histone deacetylase (HDAC) 1 and 2: complex co-stars with multiple leading parts. *Biochem. Soc. Trans.*, **41**, 741–749.
54. Li,Y. and Seto,E. (2016) HDACs and HDAC inhibitors in cancer development and therapy. *Cold Spring Harb. Perspect. Med.*, **6**, a026831.
55. Sirbu,B.M., Couch,F.B., Feigerle,J.T., Bhaskara,S., Hiebert,S.W. and Cortez,D. (2011) Analysis of protein dynamics at active, stalled, and collapsed replication forks. *Genes Dev.*, **25**, 1320–1327.
56. Miller,K.M., Tjeertes,J.V., Coates,J., Legube,G., Polo,S.E., Britton,S. and Jackson,S.P. (2010) Human HDAC1 and HDAC2 function in the DNA-damage response to promote DNA nonhomologous end-joining. *Nat. Struct. Mol. Biol.*, **17**, 1144–1151.
57. Sanchez,A., De Vivo,A., Uprety,N., Kim,J., Stevens,S.M. Jr and Kee,Y. (2016) BMI1-UBR5 axis regulates transcriptional repression at damaged chromatin. *Proc. Natl. Acad. Sci. U.S.A.*, **113**, 11243–11248.
58. Cohen,S., Puget,N., Lin,Y.L., Clouaire,T., Aguirrebengoa,M., Rocher,V., Pasero,P., Canitrot,Y. and Legube,G. (2018) Senataxin resolves RNA:DNA hybrids forming at DNA double-strand breaks to prevent translocations. *Nat. Commun.*, **9**, 533.
59. Cristini,A., Groh,M., Kristiansen,M.S. and Gromak,N. (2018) RNA/DNA hybrid interactome identifies DXH9 as a molecular player in transcriptional termination and R-loop-associated DNA damage. *Cell Rep.*, **23**, 1891–1905.
60. Marchena-Cruz,E., Camino,L.P., Bhandari,J., Silva,S., Marqueta-Gracia,J.J., Amdeen,S.A., Guillen-Mendoza,C., Garcia-Rubio,M.L., Calderon-Montano,J.M., Xue,X. *et al.* (2023) DDX47, MeCP2, and other functionally heterogeneous factors protect cells from harmful R loops. *Cell Rep.*, **42**, 112148.
61. Perez-Calero,C., Bayona-Feliu,A., Xue,X., Barroso,S.I., Munoz,S., Gonzalez-Basallote,V.M., Sung,P. and Aguilera,A. (2020) UAP56/DDX39B is a major cotranscriptional RNA–DNA helicase that unwinds harmful R loops genome-wide. *Genes Dev.*, **34**, 898–912.
62. Chang,E.Y., Tsai,S., Aristizabal,M.J., Wells,J.P., Coulombe,Y., Busatto,F.F., Chan,Y.A., Kumar,A., Dan Zhu,Y., Wang,A.Y. *et al.* (2019) MRE11-RAD50-NBS1 promotes Fanconi Anemia R-loop suppression at transcription-replication conflicts. *Nat. Commun.*, **10**, 4265.
63. Okamoto,Y., Abe,M., Itaya,A., Tomida,J., Ishiai,M., Takaori-Kondo,A., Taoka,M., Isobe,T. and Takata,M. (2019) FANCD2 protects genome stability by recruiting RNA processing enzymes to resolve R-loops during mild replication stress. *FEBS J.*, **286**, 139–150.